OXFORD

Cerebral Cortex, March 2017;27:2226–2248

doi:10.1093/cercor/bhw075
Advance Access Publication Date: 21 March 2016
Original Article

ORIGINAL ARTICLE

eEF2K/eEF2 Pathway Controls the Excitation/Inhibition Balance and Susceptibility to Epileptic Seizures

Christopher Heise[1,†], Elham Taha[2,3,†], Luca Murru[1,†], Luisa Ponzoni[4], Angela Cattaneo[5], Fabrizia C. Guarnieri[6], Caterina Montani[1], Adele Mossa[1], Elena Vezzoli[1,4], Giulio Ippolito[1], Jonathan Zapata[1], Iliana Barrera[2,3], Alexey G. Ryazanov[7], James Cook[8], Michael Poe[8], Michael Rajesh Stephen[8], Maksym Kopanitsa[9,10], Roberta Benfante[1,4], Francesco Rusconi[4], Daniela Braida[4], Maura Francolini[1,4], Christopher G. Proud[11,12], Flavia Valtorta[6], Maria Passafaro[1,4], Mariaelvina Sala[1,4], Angela Bachi[5], Chiara Verpelli[1,4], Kobi Rosenblum[2,3] and Carlo Sala[1,4]

[1]CNR Neuroscience Institute, Milan, Italy, [2]Sagol Department of Neurobiology and, [3]Center for Gene Manipulation in the Brain, Natural Science Faculty, University of Haifa, Haifa, Israel, [4]Department of Medical Biotechnology and Translational Medicine, Università degli Studi di Milano, Milan, Italy, [5]IFOM-FIRC Institute of Molecular Oncology, Milan, Italy, [6]Division of Neuroscience, San Raffaele Scientific Institute and Vita-Salute University, Milan, Italy, [7]The Department of Pharmacology, University of Medicine and Dentistry of New Jersey, Robert Wood Johnson Medical School, Piscataway, NJ 08854, USA, [8]Department of Chemistry and Biochemistry, University of Wisconsin-Milwaukee, Milwaukee, WI, USA, [9]Synome, Babraham Research Campus, Cambridge CB22 3AT, UK, [10]Charles River Discovery Research Services, 70210 Kuopio, Finland, [11]University of Southampton, Centre for Biological Sciences, Southampton SO17 1BJ, UK and [12]South Australian Health and Medical Research Institute and University of Adelaide, Adelaide, Australia

Address correspondence to Carlo Sala, CNR Neuroscience Institute, Via Vanvitelli 32, 20129 Milano, Italy. Email: c.sala@in.cnr.it

[†]These authors contributed equally.

Abstract

Alterations in the balance of inhibitory and excitatory synaptic transmission have been implicated in the pathogenesis of neurological disorders such as epilepsy. Eukaryotic elongation factor 2 kinase (eEF2K) is a highly regulated, ubiquitous kinase involved in the control of protein translation. Here, we show that eEF2K activity negatively regulates GABAergic synaptic transmission. Indeed, loss of eEF2K increases GABAergic synaptic transmission by upregulating the presynaptic protein Synapsin 2b and α5-containing $GABA_A$ receptors and thus interferes with the excitation/inhibition balance. This cellular phenotype is accompanied by an increased resistance to epilepsy and an impairment of only a specific hippocampal-dependent fear conditioning. From a clinical perspective, our results identify eEF2K as a potential novel target for antiepileptic drugs, since pharmacological and genetic inhibition of eEF2K can revert the epileptic phenotype in a mouse model of human epilepsy.

Key words: epilepsy, fear conditioning, GABA receptors, hippocampus, inhibitory synapses, translation elongation regulation

Introduction

Dynamic control of mRNA translation is crucial for proteome remodeling in neurons during synaptic plasticity and synapse formation/development and has been shown to have a profound effect on signal transmission at the chemical synapse (Sutton et al. 2006; Park et al. 2008; Holt and Schuman 2013; Nosyreva et al. 2013). Not surprisingly, several initiation and elongation factors that can regulate mRNA translation of critical synaptic proteins and synaptic plasticity processes have been identified (Costa-Mattioli et al. 2007; Gkogkas et al. 2010; Autry et al. 2011; Zhu et al. 2011; Heise et al. 2014; Ounallah-Saad et al. 2014; Sala and Segal 2014).

eEF2K, previously known as calcium/calmodulin-dependent protein Kinase III (CaMKIII), is a ubiquitous protein kinase involved in the control of mRNA translation whose catalytic activity is Ca^{2+} dependent. Upon activation, eEF2K phosphorylates and inhibits eukaryotic elongation factor 2 (eEF2), leading to inhibition of mRNA translation at the level of elongation (Ryazanov et al. 1988; Browne and Proud 2002). In neurons, eEF2K is mainly activated by an increase in Ca^{2+} levels following *N*-methyl-D-aspartate receptor (NMDAR) activation, but has also been shown to be activated by metabotropic glutamate receptors (mGluRs) (Park et al. 2008; Verpelli et al. 2010) and 5′ AMP-activated protein kinase (AMPK) (Ma et al. 2014; Kenney, Sorokina, et al. 2015). Changes in eEF2K activity are associated with modifications in the synaptic proteome and plasticity both in vitro and in vivo (Scheetz et al. 1997, 2000; Sutton et al. 2007; Park et al. 2008; Nosyreva et al. 2013). Interestingly, even though eEF2 phosphorylation is related to a decrease in general mRNA translation in neurons, it is also associated with increased expression of selected proteins in the vicinity of the synapse, though the mechanism(s) underlying this phenomenon are poorly understood (Scheetz et al. 2000; Belelovsky et al. 2005; Davidkova and Carroll 2007; Park et al. 2008; Nosyreva et al. 2013). Recently, it has been suggested that in the *Aplysia* model eEF2 acts as a biochemical sensor that is capable of bidirectionally decoding two different neuronal activity patterns, leading to differential protein synthesis and synaptic plasticity (McCamphill et al. 2015).

The regulation of translation elongation and in particular the phosphorylation of eEF2 play a role in learning and memory processes. Interestingly, eEF2 phosphorylation can either be increased following novel taste learning in the Insular Cortex (IC) (Belelovsky et al. 2005, 2009; Gildish et al. 2012) or decreased following fear-conditioning training in the hippocampus (Im et al. 2009). Genetically engineered eEF2K knock-in (KI) mice containing a point mutation in the catalytic domain of eEF2K, which markedly decreases eEF2K activity, are impaired in some forms of cortical-dependent learning (Gildish et al. 2012; Taha et al. 2013).

Despite the enlightening work on eEF2K, the role of its activity on the functionality of the chemical synapse has not been fully addressed. In addition, a complete understanding of the role of the eEF2K/eEF2 pathway in synapses and neural networks is still lacking.

Therefore, we decided to analyze the functional and proteomic effects of chronic elevation or the absence of eEF2K activity on neuronal and network processes, synapses, and synaptic events such as signal transmission at the GABAergic and glutamatergic synapse. Using in vitro and in vivo models, we found that eEF2K activity strongly impairs GABAergic signaling. Consistently, eEF2K-KO mice exhibit a stronger GABAergic transmission and tonic inhibition and are less susceptible to epileptic seizures. Genetic or pharmacological inhibition of eEF2K in a mouse model of epilepsy can rescue the epileptic phenotype. eEF2K-KO mice also display some hippocampal-dependent behavior impairments but normal cortex and amygdala-dependent behavior. This suggests that chronic manipulation of the eEF2K pathway affects specific neuronal subtypes/circuits and provides novel insights into the intimate connections between translation regulation, the inhibition/excitation ratio, and ultimately brain function.

Materials and Methods

Animals

We used 2 different eEF2K knock-out mice with a C57Bl6 background, one kindly provided by Alexey G. Ryazanov (Ryazanov 2002) and the second generated by the laboratory of Christopher Proud (Moore et al. 2015). eEF2K-KO and Syn I mice were re-derived on a C57BL/6 background (Charles River Laboratories, Calco, Italy). By using heterozygous mice for breeding, we derived wild-type (eEF2K WT) and knock-out (eEF2K-KO) littermates. The Synapsin 1 KO mice (Chin et al. 1995) were provided by Valtorta's laboratory and crossed with the eEF2K-KO mice to obtain male double KOs (eEF2K-KO+Syn1-KO) and wild-type littermates.

For primary neuronal rat cultures, we used pregnant female Sprague Dawley rats purchased from Charles River (Charles River Laboratories). For genotyping of mice, DNA was extracted from tails and analyzed by PCR as previously described (Gitler et al. 2004; Autry et al. 2011). Mice and rats were housed under constant temperature (22 ± 1°C) and humidity (50%) conditions with a 12 h light/dark cycle and were provided with food and water ad libitum. For biochemical and electrophysiological analysis of eEF2K-KO mice, male littermates between postnatal day (P) 30–42 were used (up to P120 in the case of proteomic analysis of cortex), whereas for electroencephalography (EEG) and behavioral analysis, P90–P120 mice were used. All experiments involving animals followed protocols in accordance with the guidelines established by the European Communities Council and the Italian Ministry of Health (Rome, Italy). Experimental procedures of EEG and behavioral analysis followed the guidelines established by the Italian Council on Animal Care and were approved by the Italian Government decree No. 17/2013. For experiments performed in Haifa, mice were maintained on a 12 h light/dark cycle and in a temperature-controlled room. The behavioral tests were performed during daylight hours. All animals were handled in accordance with the University of Haifa regulations and the National Institutes of Health Guidelines (Publication Number 8023). All efforts were made to minimize the number of subjects used and their suffering.

Neuronal Cultures

Primary rat and mouse neuronal cultures were prepared similarly to a previously described study (Verpelli et al. 2010) with slight modifications. Hippocampal or cortical neuron cultures were prepared from embryonic day (E) 18 rat embryos or E 17.5 mouse embryos. Neurons were plated at medium density (200 cells/mm²) on 12-well plates (Euroclone) with or without coverslips (VWR), coated with 0.01 mg/mL poly-L-Lys (Sigma-Aldrich), and cultured using home-made B27, which represents a slight variation of a

previously described formula (Chen et al. 2008) since we used a final medium concentration of 2.5 µg/mL of Apo-Transferrin (Sigma) instead of 5 µg/mL of HOLO-Transferrin. Every week (at DIV 4, 11, and 18), 40% of the volume was aspired and replaced by fresh medium (volume: 50% of the original volume). Twelve-well plates without coverslips were used for protein biochemical analysis, whereas 12-well plates with coverslips were used for immunofluorescence or electrophysiological analysis.

DNA Constructs and Lentiviral Production and Infection of Primary Neuronal Cultures

GFP, eEF2K, eEF2Kca, Syn2, and shSyn2b lentiviral constructs were previously described (Verpelli et al. 2010) or subcloned and are expressed by the previously described second generation lentiviral transfer vector FUW (Lois et al. 2002). Genetically modified lentiviruses were produced as previously described (Naldini et al. 1996; Lois et al. 2002), and the production was carried out with second- and third-generation lentiviral transfer vectors. Unless otherwise indicated, lentiviral infection took place at DIV 1. shRNASyn2b#1 was cloned into pSUPER and then subcloned into a third-generation lentivirus (pLVTHM) and exhibits the following targeting nucleotide sequence: 5′-GCATTGCAGTAGGTC CAAAAC-3′. shRNASyn2b#2 was cloned into pSUPER and then subcloned into a third-generation lentivirus (pLVTHM) and exhibits the following targeting nucleotide sequence: 5′-GCAACAAC TACAAGGCTTACA-3′.

Electrophysiology, Intracellular Recordings

For primary rat/mouse neuronal cultures, whole-cell patch-clamp recordings were performed at room temperature from DIV 20 primary cortical or hippocampal neurons perfused with external solution containing (in mM): 130 NaCl, 2.5 KCl, 2.2 $CaCl_2$, 1.5 $MgCl_2$, 10 D-glucose, 10 HEPES-NaOH (pH 7.4; osmolarity adjusted to 290 mOsm) for mIPSCs or Krebs'–Ringer's–HEPES solution containing (in mM): 125 NaCl, 5 KCl, 1.2 $MgSO_4$, 1.2 KH_2PO_4, 2 $CaCl_2$, 6 glucose, and 25 HEPES (pH 7.4) for mEPSCs. For mPSC recordings, blockers of voltage-dependent sodium channels (500 µM lidocaine) were included in the extracellular solution. This was done in combination with blockers for $GABA_A$Rs (20 µM bicuculline) or blockers for NMDARs, AMPARs/Kainate receptors (3 mM Kynurenic acid [KYN]) for mEPSC or mIPSC recordings, respectively. The composition of the intracellular solution was (in mM)126 K-gluconate, 4 NaCl, 1 EGTA, 1 $MgSO_4$, 0.5 $CaCl_2$, 3 ATP (magnesium salt), 0.1 GTP (sodium salt), 10 glucose, 10 HEPES-KOH (pH 7.3; osmolarity adjusted to 280 mOsm) for mEPSCs recordings or 140 mM CsCl, 2 mM $MgCl_2$, 1 mM $CaCl_2$, 10 mM EGTA, 10 mM HEPES-CsOH, 2 mM ATP (disodium salt) (pH 7.3) for mIPSCs. Recordings were performed with a Multiclamp 700B amplifier (Axon CNS molecular devices, USA). Pipette resistance was 2–3 MΩ and series resistance was always below 20 MΩ. mEPSCs and mIPSCs were recorded at a holding potential of –70 mV over a period of 2–5 min, filtered at 2 kHz, and digitized at 20 kHz using Clampex 10.1 software. Analysis was performed offline with Clampfit 10.1 software using a threshold crossing principle. The detection level was set at 5 pA, and raw data were visually inspected to eliminate false events. Cells with noisy or unstable baselines were discarded. mEPSC and mIPSCs population averages were obtained by aligning the events at the mid-point of the rising phase. The weighted decay time constant (Dt) of mEPSCs was calculated as described (Cingolani et al. 2008).

For slices, WT and eEF2K-KO mice were anesthetized in a chamber saturated with isoflurane and then decapitated. The brain was rapidly removed and placed in an ice-cold solution containing 220 mM sucrose, 2 mM KCl, 1.3 mM NaH_2PO_4, 6 mM $MgCl_2$, 0.2 mM $CaCl_2$, 10 mM glucose, 2.6 mM $NaHCO_3$ (pH 7.3, equilibrated with 95% O_2 and 5% CO_2), and 3 mM KYN. Coronal hippocampal slices (thickness, 250–300 µm) were prepared with a vibratome VT1000 S (Leica) and then incubated first for 40 min at 36°C and then for 30 min at room temperature in artificial CSF (aCSF), consisting of (in mM) 125 NaCl, 2.5 KCl, 1.25 NaH_2PO_4, 1 $MgCl_2$, 2 $CaCl_2$, 25 glucose, and 26 $NaHCO_3$ (pH 7.3, equilibrated with 95% O_2 and 5% CO_2). Slices were transferred to a recording chamber perfused with aCSF at 33°C temperature at a rate of about 2 mL/min. Whole-cell patch-clamp electrophysiological recordings were performed with a Multiclamp 700B amplifier (Axon CNS molecular devices, USA) using an infrared differential interference contrast microscope. Patch microelectrodes (borosilicate capillaries with a filament and an outer diameter of 1.5 µm; Sutter Instruments) were prepared with a 4-step horizontal puller (Sutter Instruments) and had a resistance of 3–5 MΩ. Tonic GABAergic currents were recorded at a holding potential of –65 mV with an internal solution containing 140 mM CsCl, 2 mM $MgCl_2$, 1 mM $CaCl_2$, 10 mM EGTA, 10 mM HEPES, 2 mM ATP (disodium salt) (pH 7.3 with CsOH), and 5 mM QX-314 (lidocaine *N*-ethyl bromide). Access resistance was between 10 and 20 MΩ; if it changed by >20% during the recording, the recording was discarded. All GABAergic currents were recorded in the presence of KYN (3 mM) in the aCSF. For recordings of tonic currents, after a baseline period of 2–5 min, GABA (5 µM), muscimol (50 nM or 5 µM), or THIP (3 µM) were added for approximately 5 min to the aCSF to increase the tonic component of the GABAergic transmission and to understand whether there were modification in efficacy of extrasynaptic $GABA_A$Rs. In fact, THIP, at the used concentration, acts preferentially activating extrasynaptic δ subunit-containing $GABA_A$R. To study α_5, containing $GABA_A$Rs, L-655,708 (100 nM), which acts as an inverse agonist at the benzodiazepine binding site preferentially on the α_5 subunit-containing $GABA_A$Rs, was co-applied with muscimol (50 nM). At the end of the experiments, Bic (20 µM) was added to block all GABAergic currents. For the recording of mIPSCs, lidocaine (500 µM) was added in the external solution. Granule cell-evoked IPSCs (eIPSCs) were elicited with a patch pipette placed near the patched neuron in the molecular layer of the dentate gyrus. Pairs of stimuli were delivered at 70-ms intervals every 20 s (frequency of 0.05 Hz), and PPRs were calculated by dividing the amplitude of the second response by the first one. Currents were filtered at 2 kHz and digitized at 20 kHz using Clampex 10.1 software. Analysis was performed offline with Clampfit 10.1 software.

Electrophysiology, Extracellular Recordings

Preparation of Hippocampal Slices for Field Potential Measurements on Multi-electrode Arrays

Slice preparation procedures were performed as previously described (Kopanitsa et al. 2006). In brief, mice were sacrificed by cervical dislocation and the brain immediately immersed in ice-cold "cutting" solution (110 mM sucrose, 60 mM NaCl, 28 mM $NaHCO_3$, 1.25 mM NaH_2PO_4, 3 mM KCl, 7 mM $MgSO_4$, 0.5 mM $CaCl_2$, 5 mM glucose, 1.5 µM phenol red) gassed with a gas mixture of 95%O_2/5%CO_2. Whole brain slices were cut at 350 µm thickness by a Vibroslice MA752 (Campden Instruments, Loughborough, UK) with the blade set at an angle of 20–30 °C to the horizontal planes of the brain. "Cutting" solution in a temperature-controlled Peltier bath was maintained at 0–3 °C and constantly saturated with a mixture of 95% O_2 and 5% CO_2. Up to 8 slices containing medial segments of the hippocampus with overlaying cortical areas were trimmed of

the remaining tissue, placed into a well of a slice chamber (Fine Science Tools, Foster City, CA, USA) and kept interfaced between moist air and subfused fresh artificial cerebrospinal fluid (ACSF) containing 124 mM NaCl, 25 mM $NaHCO_3$, 1 mM NaH_2PO_4, 4.4 mM KCl, 1.2 mM $MgSO_4$, 2 mM $CaCl_2$, 10 mM glucose, and 1.5 µM phenol red. Temperature in the chamber was slowly increased to 30 °C for the rest of the incubation time. Slices were incubated in these conditions for at least 2–3 h before experiments commenced.

fEPSP recordings. Field excitatory postsynaptic potentials (fEPSPs) were recorded by the MEA60 electrophysiological suite (Multi Channel Systems, Reutlingen, FRG). Four set-ups consisting of a MEA1060-BC pre-amplifier and a filter amplifier (gain 550×) were run simultaneously by a data acquisition unit operated by MC_Rack software. Raw electrode data were digitized at 10 kHz and stored on a PC hard disk for subsequent analysis. To record fEPSPs, a hippocampal slice was placed into the well of a 5 × 13 3D multi-electrode array (MEA) biochip (Ayanda Biosystems, Lausanne, Switzerland). The slice was guided to a desired position with a fine paint brush and gently fixed over MEA electrodes by a silver ring with attached nylon mesh lowered vertically by a 1-dimensional U-1C micromanipulator (You Ltd, Tokyo, Japan). MEA biochips were fitted into the pre-amplifier case, and fresh ACSF was delivered to the MEA well through a temperature-controlled perfusion cannula that warmed perfused media to 32 °C. Monopolar stimulation of Schaffer collateral/commissural fibers through array electrodes was performed by a STG4008 stimulus generator (Multi Channel Systems, Reutlingen, FRG). Biphasic (positive/negative, 100 µs/a phase) voltage pulses were used. Amplitude, duration, and frequency of the stimulation were controlled by MC_Stimulus II software.

All LTP experiments were done using 2-pathway stimulation of Schaffer collateral/commissural fibers (Schwartzkroin and Wester 1975; Andersen et al. 1977). Previous experiments that utilized MEAs demonstrated that the largest LTP was recorded in the proximal part of apical dendrites of CA1 pyramidal neurons (Kopanitsa et al. 2006). Therefore, a single principal recording electrode was picked in the middle of the proximal part of CA1 and assigned 2 electrodes for stimulation of the control and test pathways on the subicular side and on the CA3 side of the SR, respectively. The distance from the recording electrode to the test stimulation electrode was 420–510 µm and the distance to the control stimulation electrode was 316–510 µm.

Spontaneous network oscillations. A similar 4× MEA60 electrophysiological suite was used for parallel recordings of spontaneous oscillations of field potential evoked by 100 nM kainate in the CA3 area of ventral hippocampal slices. To increase signal-to-noise ratio, oscillations were recorded using 8 × 8 200 3D MEA biochips (Ayanda Biosystems) with slightly larger electrodes compared with 5 × 13 3D MEA biochips used for evoked fEPSP recordings. Raw electrode data were digitized at 2 kHz and stored on a PC hard disk for subsequent analysis using Spike2 software (v. 7.04, Cambridge Electronic Design Ltd, Cambridge, UK).

Electrophysiological Data Analysis.

Analysis of fEPSP recordings. To evoke orthodromic fEPSPs, stimulation electrodes were activated at a frequency of 0.02 Hz. Amplitude or 20–80% slope of the negative part of fEPSPs was used as a measure of the synaptic response. Following at least 10–15 min of equilibration inside an MEA well, I/O relationships were obtained and baseline stimulation strength was set to evoke a response that corresponded to approximately 40% of the maximal attainable fEPSP at the principal recording electrode. PPF was observed after stimulating Schaffer collateral/commissural fibers with a pair of pulses at baseline stimulation strength and an interpulse interval of 50 ms. PPF value was calculated as $fEPSP_2/fEPSP_1 \times 100\%$. Average data from 5 paired pulse stimulations were used for each slice. LTP was induced after a 60 min period of stable baseline responses by one of the 2 induction protocols:

1. theta-burst stimulation (TBS) train consisting of 10 bursts given at 5 Hz with 4 pulses given at 100 Hz per burst
2. 2 trains of 1 s long high-frequency 100 Hz stimulation (HFS)

Stimulus strength was not altered during LTP induction. LTP plots were scaled to the average of the first 5 baseline points. To account for a possible drift of baseline conditions, slope values in the test pathway were normalized by slope amplitudes in the control pathway prior to statistical comparison. LTP magnitude was assessed by averaging normalized fEPSPs in the test pathway 180–185 min after LTP induction.

To assess changes in basal synaptic transmission, input–output relationships were initially compared by mixed model repeated-measures ANOVA and Bonferroni post hoc tests implemented in Prism 5 (GraphPad Software, Inc., San Diego, CA, USA) using individual slice data as independent observations. Since several slices were routinely recorded from every mouse, fEPSP-max, PPF, and LTP values between wild-type and mutant mice were then compared using 2-way nested ANOVA design with genotype (group) and mice (subgroup) as fixed factors (STATISTICA v. 10, StatSoft, Inc., Tulsa, OK, USA). The main genotype effect was considered to be significant if $P < 0.05$.

Analysis of spontaneous network oscillations. Spontaneous network oscillations were activated by the application of 100 nM kainate [4]. Most of the slices did not display a clear oscillatory pattern of extracellular field potentials before the incubation with the drug, although about 30% of the slices exhibited baseline oscillatory activity in the theta range (3–7 Hz). Over the first 15 min of incubation with kainate, approximately 60% of the slices started to display sustained high-frequency oscillations with the dominant frequencies in the β/γ range (15–35 Hz). The power of such oscillations stabilized after 30 min and remained stable for another 30–45 min. The remaining approximately 40% of ventral hippocampal slices displayed rhythmic low-frequency seizure-like phasic discharges (up to 1–2 Hz) in response to incubation with kainate while sustained high-frequency β/γ oscillations were absent.

Oscillation power was calculated by fast Fourier transforms over 60–90 s continuous recordings (Hanning window, FFT size 2048). Peak values of the power spectrum, as well as the respective dominant frequency of synchronous activity recorded by 1 MEA electrode at which oscillation power was maximal in a given slice, were selected for statistical analysis. Slices in which peak power values were lower than 1 μV^2 were excluded from further analysis. To analyze differences in the peak power values and dominant oscillation frequencies, mixed-model repeated-measures ANOVA and Bonferroni post hoc tests implemented in Prism 5 were used (GraphPad Software, Inc.), using individual slice data as independent observations. Since the distribution of peak power values significantly deviated from normality, these data were $\log_{10}$ transformed prior to ANOVA.

Graph plots and normalizations were performed using OriginPro 8.5 (OriginLab, Northampton, MA, USA). Data were presented as mean ± SEM with n and N indicating the number of slices and mice, respectively. All analyses were performed blindly without the researcher knowing the genotype of the mice.

Real-Time Polymerase Chain Reaction

Total messenger RNA (mRNA) was analyzed by Real-time polymerase chain reaction (qRT-PCR). Total RNA was extracted from primary rat cortical cultures infected with GFP or eEF2Kca at DIV 20, using the RNeasy Mini Kit and accompanying QIAshredder (Qiagen) according to the manufacturer's instructions. Contaminating DNA in the sample was degraded by on-column incubation with DNaseI (Qiagen) for 15 min. One microgram per sample was reverse-transcribed using SuperScript III (Life Technologies, Inc.) in accordance with the manufacturer's instructions. Gene expression was quantitatively analyzed by amplification carried out with the ABI Prism 7000 Sequence Detection System and SDS software version 1.2.3 (Applied Biosystems, Inc., CA, USA). The target sequences were amplified from 50 ng of cDNA in the presence of TaqMan Gene Expression Master Mix (Life Technologies, Inc.). The TaqMan™ primer and probe assays (Life Technologies, Inc.) were eEF2 (ID # Rn00820849_g1), MAP1b (ID # Rn01399486_m1), TRIM3 (ID # Rn01509048_m1), Slc32a1 (namely VGAT, ID # Rn00824654_m1), Syn2 (ID # Rn00569739_m1), Gad2 (namely GAD65, ID # Rn00561244_m1), Dlg4 (namely PSD95, ID # Rn00571479_m1); glyceraldehyde-3-phosphate dehydrogenase (GADPH; ID # Rn99999916_s1) was used as endogenous control. All assays were tested and confirmed as compatible for use with GAPDH as an endogenous control. The $2^{-\Delta\Delta CT}$ method was used to calculate the results, thus allowing the normalization of each sample to the endogenous control, and comparison with the calibrator for each experiment (set to a value of 1), as described in the figure legends.

Protein Biochemistry

Cultured neurons or brain homogenates were collected with precooled "buffered sucrose" (0.32 M sucrose [Sigma-Aldrich]/4 mM HEPES-NaOH buffer [Sigma-Aldrich], pH 7.3, protease inhibitors [Roche]) and analyzed via Bradford protein assay (Bio-Rad) before the addition of loading dye (250 mM Tris, 8% [w/v], 40% [v/v] glycerol, 0.008% [w/v] bromophenol blue [all Sigma-Aldrich]). In some cases, fractionation took place prior to Bradford protein assay analysis, which resulted in a P1 fraction (enriched in cell bodies and dendritic fragments) and a P2 fraction (enriched in presynaptic and postsynaptic components) (Huttner et al. 1983; Grabrucker et al. 2011). Twenty micrograms of samples were loaded in the pockets of 6–15% polyacrylamide gels followed by electroblotting onto a nitrocellulose membrane. Primary antibodies were applied for 3 h in blocking buffer (TBS-T and 5% dried nonfat milk). For cell culture lysates, chemoluminescence was evoked using HRP-conjugated secondary antibodies and an ECL kit (GE Healthcare) or using fluorophore coupled secondary antibodies (LI-COR), detection via Odyssey scanner (LI-COR). The SUnSET method was performed as described in Hoeffer et al. (2011); Santini et al. (2013). Immunoblot bands intensity was quantified manually with ImageJ (US National Institutes of Health) on samples of groups run adjacently to each other by a blinded independent investigator. Loading control and normalization took place via actin, an appropriate loading control/normalization for biochemical fractions enriched in synaptic compartments as the primary cytoskeletal element at synapses is actin (Schmeisser et al. 2012). For the SUNSET experiments, blue Coomassie staining quantification was also performed. For practical reasons, blots were cut before antibody incubation, and therefore, proteins with sufficiently different molecular weights could be analyzed in 1 blot. Actin loading control for WB displayed in Figures 3 and 4, Supplementary Figures 3, 4, and 7 is shown in Supplementary Figure 14.

Antibodies

The following primary antibodies were used (dilution and sources): mouse anti (β-) actin (1:1000, Sigma-Aldrich), rabbit anti Caspase-3 (1:1000, Cell Signalling), rabbit anti eEF2 (1:400, Cell Signalling), rabbit anti eEF2K (1:400, Cell Signalling), rabbit anti eEF2K (1:50, Thermo Scientific), mouse anti $GABA_AR\alpha1$ (1:1000 WB, 1:500 IF, NeuroMab), mouse anti $GABA_AR\alpha5$ (1:250 WB, Abcam), mouse anti GAD65 (1:500, Abcam), mouse anti GFP (1:1000, Roche), rabbit anti GluA1 (1:1000 WB, 1:200 IF, Millipore), rabbit anti MAP1b (1:1500, Proteintech), mouse anti MAP2 (1:400, Abcam), mouse anti NLGN1 (1:10000, NeuroMab), rabbit anti peEF2 (1:500, Cell Signalling), mouse anti PSD95 (1:5000 WB, 1:400 IF, NeuroMab), mouse anti Syp (1:200, Sigma-Aldrich), mouse anti Syn (Vaccaro et al. 1997) (1:1000, gift from Dr F. Valtorta [Division of Neuroscience, San Raffaele Scientific Institute and Vita-Salute University, Milan, Italy]), mouse anti Syn2 (1:1000, gift from Prof. Fabio Benfenati [University of Genova, Genova, Italy]), rb anti Syn 1/2 (1:400, Synaptic Systems), rabbit anti TRIM3 (1:200, Abcam), mouse anti (α-)tubulin (1:1000, Sigma-Aldrich), rabbit anti VGAT, and anti VGLUT1 (1:200, Synaptic Systems). Secondary anti-mouse and anti-rabbit antibodies, conjugated with peroxidase, FITC, Cy3, or Cy5 were purchased from Jackson Immuno Research Laboratories; anti-mouse IgG, 680RD, and anti-rabbit IgG, 800RD were purchased from LI-COR.

Electron Microscopy

Mice were anesthetized by intraperitoneal injection of 10 mg/mL avertine and transcardially perfused with 2.5% glutaraldehyde, 2% paraformaldehyde in 0.15 M sodium cacodylate buffer pH 7.4. Dissected brains were post-fixed for additional 24 h at 4 °C. Coronal sections (100 µm thickness) were obtained with a vibratome (Leica VT1000S), and hippocampi were manually dissected. After washing, samples were post-fixed with 2% osmium tetroxide, rinsed, stained with 1% uranyl acetate in water for 45 min, dehydrated, and embedded in epoxy resin (Electron Microscopy Science, Hatfield, PA, USA) that was baked for 48 h at 60°C. Thin sections were obtained with an ultramicrotome (Leica Microsystems, Austria) and observed under a Philips CM10 transmission electron microscopy (TEM) (FEI, Eindhoven, the Netherlands). For quantitative analyses, images were acquired at a final magnification of 25–34 000 using a Morada CDD camera (Olympus, Munster, Germany).

For immuno-EM analysis, according to the conventional protocol for sample preparation, tissue blocks from the molecular layer of the dentate gyrus were cut in a Leica EM UC6 ultramicrotome. Ultrathin sections (70–90 nm) were collected on formvar carbon-coated nickel grids and processed for GABA immunolabeling as follows: after a 5 min incubation in TBST pH 7.6 (Tris–HCl 0.05 M, pH 7.6, with 0.9% NaCl and 0.1% Triton X-100), grids were incubated with rabbit antiserum against GABA (Sigma A2052, 1:10.000 in TBST) overnight in a moist chamber at RT. Grids were then washed twice for 5 min and once for 30 min in TBST pH 7.6. After 5 min of conditioning in TBST pH 8.2 (0.05 M Tris, pH 8.2, with 0.9% NaCl, and 0.1% Triton X-100), grids were incubated for 2 h in goat anti-rabbit IgG conjugated to 10 nm colloidal gold (Aurion, the Netherlands) diluted 1:25 in TBST pH 8.2. They were then washed twice in TBST pH 7.6, rinsed in deionized water, allowed to air-dry, and counterstained with 1% uranyl acetate and 1% lead citrate. Images of GABA-immunopositive synaptic terminals were taken at a magnification of ×25 000, and quantitative analyses were performed with ImageJ 1.47v.

For quantitative analysis of TEM images, the following values were evaluated: synaptic vesicle (SV) density and area of

presynaptic terminals; for excitatory synapses, the number of docked vesicles and the length and thickness of the PSDs were also evaluated. The number of inhibitory synapses was determined by counting the number of GABAergic synapses per micrometer of neuron soma perimeter measured on images acquired at low magnification. Images were analyzed with ImageJ1.47v (NIH Image) by a blinded independent investigator. All data were presented as mean ± SEM. For each group of data, an F-test for the comparison of the variances was used before the statistical analysis. In case of nonhomogeneity of variance, the statistical analysis was performed using the nonparametric Welch's *t*-test for unequal variances. In the case of equal variances, 2-tailed unpaired Student's *t*-test was used.

Electroencephalography Analysis

WT, eEF2K-KO, Syn1-KO, and eEF2K/Syn1-DKO mice were anesthetized with an i.p. injection of 5% chloral hydrate dissolved in saline and given at a volume of 10 mL/kg. Four screw electrodes (Bilaney Consultants GMBH, Dusseldorf, Germany) were inserted bilaterally through the skull over the cortex (anteroposterior, +2.0–3.0 mm; left–right 2.0 mm from bregma) as previously described (Manfredi et al. 2009) according to brain atlas coordinates (Franklin and Paxinos 2008); a further electrode was placed into the nasal bone as ground. The 5 electrodes were connected to a pedestal (Bilaney, Dusseldorf, Germany) and fixed with acrylic cement (Palavit, New Galetti and Rossi, Milan, Italy). The animals were allowed to recover for a week from surgery before the experiment. After surgery, EEG activity was recorded in a Faraday chamber using a Power-Lab digital acquisition system (AD Instruments, Bella Vista, Australia; sampling rate 100 Hz, resolution 0.2 Hz) in freely moving awake mice. Basal cerebral activity was recorded continuously for 22–24 h (from 5 pm to 4 pm). A quantitative analysis of spectral power was performed using fast Fourier transform. Each 2-h spectral power was calculated between 0 and 25 Hz, with a 0.2 Hz resolution, using the standard spectral power distribution: δ (0–4 Hz), θ (4.2–8 Hz), α (8.2–13 Hz), and β (13.2–25 Hz). Segments with movement artefacts or electrical noise were excluded from statistical analysis. All EEG tracings were also analyzed and scored for the presence of spikes, which were discriminated offline with the spike histogram extension of the software (LabChart v8 Pro Windows). Spikes were defined as having a duration <200 ms with baseline amplitude set to 4.5 times the standard deviation of the EEG signal (determined during inter-spike activity periods, whereas repetitive spiking activity was defined as 3 or more spikes lasting <5 s).

For susceptibility to convulsants, after 30 min of baseline, animals were given pilocarpine (300 mg/kg i.p.) or pentylenetatrazol (PTZ) (30 mg/kg i.p.) and immediately recorded for EEG activity. Atropine methylnitrate (5 mg/kg i.p.) was given 30 min before pilocarpine to reduce peripheral cholinergic side effects. Behavior and EEG traces were analyzed as previously described (Nosten-Bertrand et al. 2008) for 100 min after drug treatment. Seizures were scored as per Racine's scale (1, mouth and facial movement; 2, head nodding; 3, forelimb clonus; 4, rearing with forelimb clonus; and 5, rearing and falling with forelimb clonus). The number of animals showing seizures (Racine scale 3–5), the total number of seizures, the latency to the first seizure, and latency to death were also evaluated. In accordance with a previous study (Erbayat-Altay et al. 2008), EEG seizures were characterized as the absence (Racine scale 1–2) when associated with rhythmic 4–6 Hz sharp waves of spindle-like events; myoclonic seizures (Racine scale 3) consisting of whole body jerk and bilateral forelimb movements associated with solitary spike or polyspike and slow wave; generalized clonic or tonic seizures (Racine scale 4–5) (whole body jerks consisting of a train of spikes [clonic] or a voltage attenuation [tonic phase] which lasted 30–60 s). Rhythmic sharp waves, spikes, or polyspikes were characterized by amplitude at least 2 times higher than baseline. Seizures were video-monitored and reviewed offline by a blinded independent investigator to exactly score the seizures. Lethality was monitored within 7 days after drug injection.

Behavioral Procedures

All the behavioral scoring was performed on a blind basis by a trained experimenter.

Conditioned Taste Aversion

Conditioned taste aversion (CTA) was performed as described previously (Rosenblum et al. 1993). Saccharin (0.5% w/v; CS chemicals, Israel) was used as the novel taste in training (conditioned stimulus, CS) and injection of LiCl (0.14 M, 0.075 M, 2% body weight i.p., Sigma) as the malaise-inducing agent (unconditioned stimulus, US). At the beginning of the behavioral experiment, mice were trained for 3 days to drink out of 2 pipettes, each containing 5 mL of water, for 20 min. On the conditioning day (Day 4), the mice were allowed to drink the saccharin solution instead of water from similar pipettes for 20 min, and 40 min later were injected with LiCl. Two days following training, a multiple choice test was performed, in which mice received 4 pipettes simultaneously, 2 containing 5 mL of novel taste and 2 containing 5 mL of water. The conditioned mice preferred water to saccharin in the multiple choice test, whereas nonconditioned mice preferred saccharin to water. The aversion index was defined as [water (mL)/(water (mL) + saccharin (mL))] consumed in the test.

Familiar Object in Novel Place

The apparatus consisted of a square arena of 50 × 50 cm (Noldus Information Technology, Canada). Two objects were placed in a symmetrical position about 6 cm from the walls. Mice were habituated to the empty arena for 1 day by exploring the arena for 5 min and given 2 trials per day. After exploration, the mice were returned to the home cage. After the habituation period, the mice underwent acquisition for 2 similar objects for 5 min and given 2 trials per day for 3 days. After the acquisition period, mice were tested for familiar object recognition in a novel place, in which one of the objects was moved to a new place. The mice were allowed to explore the arena for 5 min per trial. At the beginning of each trial, the mice were placed at the center of the arena. The arena was always cleaned using 10% ethanol between trials to avoid odor effects. Exploration of the objects was defined as directing the nose or touching the object at a distance of 2 cm. Climbing the object was not considered to be exploration. Time spent exploring was measured as a percentage of exploring a familiar object in a novel place relative to the total exploration time. Animal behavior was recorded, and the data were analyzed by EthoVision XT 9 software (Noldus Information Technology, Canada).

Morris Water Maze

The Morris water maze (MWM) test was carried out as previously described (Williams et al. 2006). The MWM consisted of a black circular pool (120 cm; 50 cm) filled with water mixed with milk powder. The pool was divided into 4 quadrants. The animals learned to use distal cues to navigate a direct path to the hidden platform when placed at different, random locations around the

perimeter of the tank. During the learning period, the mice were given 4 daily trials for 4 days at 1 min per trial. To assess reference memory at the end of learning, a probe (transfer) trial was performed 24 h following the last learning trial in which the platform was removed from the pool. During the learning period, escape latency was measured in each trial. Learning curve data were presented as mean ± SEM of all 4 trials per day. Percentage of time spent in each quadrant along the entire probe test was measured, and the data were analyzed by EthoVision XT 9 software (Noldus Information Technology, Canada).

Reversal Morris Water Maze

Two days following the probe test of the standard MWM paradigm, reverse MWM tests were performed on the same animals. In this test, the platform was relocated in the opposite quadrant, and 4 trials per day were performed. Reversal learning in the MWM reveals whether or not animals can extinguish their initial learning of where the platform is positioned and learn a direct path to the new goal position. Tracking patterns typically reveal that mice swim to the previous location first and then begin to search in an arching pattern to reach the new goal. Even after multiple trials, mice do not entirely abandon their initial learning strategy and begin trials by starting to move toward the original platform position, then turn and swim more directly to the new goal. Each trial lasted for 1 min, escape latency was measured, and previous platform crossings were analyzed. The data were analyzed by EthoVision XT 9 software (Noldus Information Technology, Canada).

Trace Fear Conditioning

Training and testing were performed in a transparent cage (17.5 × 17.5 × 30 cm), placed in a sound-attenuating chamber. The cage floor consisted of 16 steel rods through which an electrical shock was delivered (Coulbourn Instruments, USA). The chamber was illuminated by a 20 W bulb.

On the conditioning day, mice were placed in the training chamber (with light, cleaned with 50% ethanol and DDW before each trial) for 120 s, followed by 7 × (20 s tone [80 dB, 2800 Hz], 20 s interval, 2 s shock [0.5 mA]). An interval of 100 s was given as a post shock period. Total time for the conditioning trial was 1220 s. Testing was performed after 24 h.

For contextual fear-conditioning tests, animals were returned to the same chamber of training 24 h after training for 300 s without tone.

For auditory fear-conditioning and trace fear-conditioning tests, animals were placed in a new context (chamber without light, black plastic floor, cleaned with 50% ethanol, and DDW before each trial, recorded with an IR camera) for 1220 s. Tone presentation (without shock) was delivered at time points identical to the conditioning trial. Animal behavior was recorded, and data were analyzed by FreezFrame 3.0 software (Coulburn Instruments, USA). The index for fear memory was freezing.

Delay Fear Conditioning

Training and testing were performed in a transparent cage (17.5 × 17.5 × 30 cm), placed in a sound-attenuating chamber. The cage floor consisted of 16 steel rods through which an electrical shock was delivered (Coulbourn Instruments, USA). The chamber was illuminated by a 20 W bulb.

On the conditioning day, mice were placed in the training chamber (with light, cleaned with 50% ethanol and DDW before each trial) for 120 s, followed by 2 × (30 s tone [80 dB, 2800 Hz], co-terminated with 1 s shock [0.7 mA]), and 30 s free stimulus interval between 2 pairings. An interval of 60 s was given as a post shock period. Total time for the conditioning trial was 270 s. Testing was performed after 24 h.

For contextual fear-conditioning tests, animals were returned to the same chamber of training 24 h after training for 300 s without tone.

For auditory fear-conditioning tests, animals were placed in new context (chamber without light, black plastic floor, cleaned with DDW before each trial, recorded with an IR camera) for 120 s followed by 3 tones like during the training period (without shock). Total time for the testing trial was 320 s. Animal behavior was recorded, and the data were analyzed by FreezFrame 3.0 software (Coulburn Instruments, USA). The index for fear memory was freezing.

Data Analysis and Display

Data were expressed as means ± SEM or percentage, analyzed for statistical significance, and displayed by Prism 5 software (GraphPad). If there were only 2 groups whose means were being compared, a Student's *t*-test was carried out to assess statistical significance (for electron microscopy, additional analyses were carried out as described in the corresponding section). For the biochemical analysis of eEF2K-KO mice (Fig. 4*D*; see Supplementary Fig. 7A), KO samples were always standardized by WT littermates run adjacently in the particular western blot. The accepted level of significance was $P \leq 0.05$. In all cases with 3 or more groups, a one factorial analysis of variance (ANOVA) was calculated for the data and if group means differed in a significant manner ($P \leq 0.05$), a post hoc Tukey test was calculated to assess statistical significance. The accepted level of significance for the post hoc test was $P \leq 0.05$.

Results

eEF2K Activity Regulates the Balance Between Excitatory and Inhibitory Synapses

To decipher whether eEF2K activity differentially affects signal transmission at the excitatory and inhibitory synapse, we first used whole-cell patch-clamp recordings to measure mPSCs. The analysis was carried out employing an in vitro eEF2K gain-of-function design (primary neuronal cultures) and an in vivo loss-of-function design (eEF2K-KO mice). Hippocampal neurons were infected at days in vitro 1 (DIV 1) with lentiviruses expressing GFP, a constitutively active form of eEF2K (eEF2Kca) (Verpelli et al. 2010) or as previously described (Pyr Dit Ruys et al. 2012), catalytically inactive form of eEF2K (K170 M). Recording took place at DIV 20. eEF2K activity markedly reduced the frequency of mEPSCs while leaving other mEPSC parameters unaffected (Fig. 1A–C). eEF2K activity also reduced the frequency of mIPSCs but also the decay time, area, and amplitude (Fig. 1A,B,D).

Instead, we observed a strong increase in the miniature inhibitory postsynaptic current (mIPSC) frequency and amplitude in hippocampal granule cells of eEF2K-KO mice, while the area only shows a trend for an increase (Fig. 1E, F,H). Despite these findings, no change in the amplitude of evoked IPSCs or in the paired pulse ratio at a short interval was observed (see Supplementary Fig. 1A). Importantly, miniature excitatory postsynaptic current (mEPSC) parameters were not different compared with WT mice (Fig. 1E–G).

To determine whether eEF2K genetic deletion affects basal synaptic transmission, extracellular recordings were performed in hippocampal slices of eEF2K-KO and WT mice. Input–output relationships as a response to stimulation of Schaffer collaterals

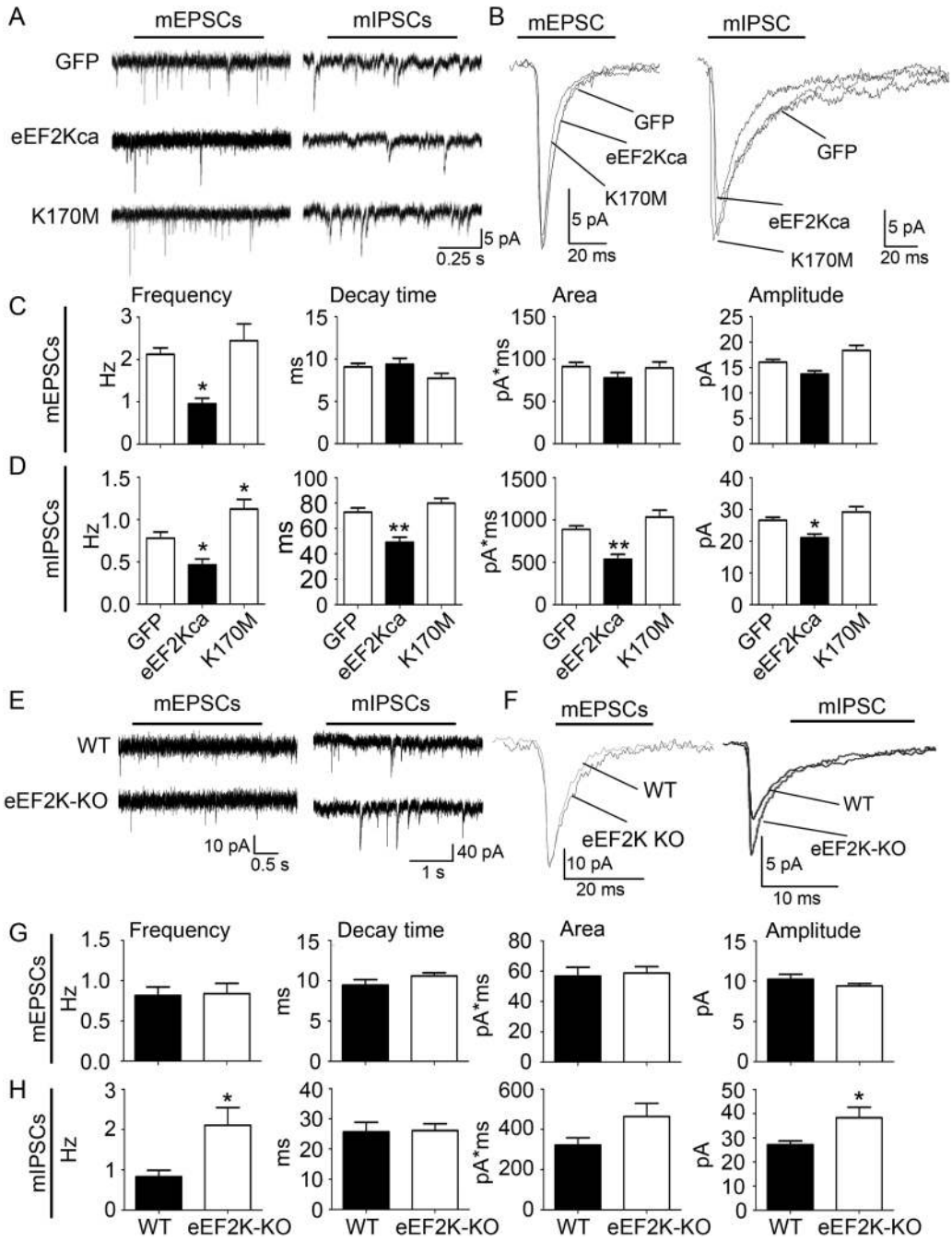

Figure 1. eEF2K activity negatively regulates GABAergic synaptic transmission. (*A*) Representative mPSC traces of GFP, eEF2Kca, or K170 M overexpressing neurons. (*B*) Representative mEPSCs and mIPSCs are shown for GFP, eEF2Kca, and K170 M. (*C*) Quantification of mESCs traces (frequency, decay time, area, and amplitude parameters) from GFP, eEF2Kca, and K170 M overexpressing neurons. Error bars are SEMs. $N = 17–30$ neurons from at least 3 cell cultures derived from different animals. $^*P < 0.05$ versus GFP (ANOVA and post hoc Tukey test). (*D*) Quantification of mISCs parameters from GFP, eEF2Kca, and K170 M overexpressing neurons. Error bars are SEMs. $N = 17–30$ neurons from at least 3 different cell cultures derived from different animals. * and $^{**}P < 0.05$ and 0.01 versus GFP (ANOVA and post hoc Tukey test). (*E*) Representative mPSC traces measured in granule cells of dentate gyrus of WT and eEF2K-KO mice. (*F*) Representative mEPSCs and mIPSCs measured in granule cells of dentate gyrus of WT and eEF2K-KO mice. (*G*) Quantification of mEPSC traces measured in dentate gyrus of WT and eEF2K-KO mice. Error bars are SEMs. $N = 13$ neurons from at least 2 different animals per group. (*H*) Quantification of mIPSC traces measured in granule cells of dentate gyrus of WT and eEF2K-KO mice. Error bars are SEMs. $N = 11$ neurons from at least 2 different animals per group. $^*P < 0.05$ versus WT (Student's *t*-test).

by biphasic voltage pulses of 0.1–4.2 V were measured in the CA1 region of the hippocampus. Representative families of fEPSP traces are given (see Supplementary Fig. 1B), indicating that baseline synaptic transmission is normal in eEF2K-KO mice compared with WT littermates.

Next, we tested long-term potentiation (LTP) induced by high-frequency stimulation (HFS) or theta-burst stimulation (TBS) in eEF2K-KO CA1 region of the hippocampus. eEF2K-KO mice exhibited normal LTP formation induced by HFS or TBS in the CA1 region. There was no significant difference in the normalized

magnitude of fEPSP slopes 180–185 min after LTP induction by 2 trains of HFS or by TBS train between eEF2K-KO and WT mice (see Supplementary Fig. 1C,D).

Paired pulse facilitation (PPF) was measured in the CA1 area of hippocampal slices of eEF2K-KO and WT mice. PPF was observed after stimulating Schaffer collateral/commissural fibers with a pair of pulses at baseline stimulation strength and an interpulse interval of 50 ms. PPF was normal in slices from eEF2K-KO animals compared with their WT littermates (see Supplementary Fig. 1E).

Since genetic deletion does not appear to affect mEPSCs or excitatory transmission, we decided to study how eEF2K activity specifically affects the GABAergic system in vivo by first measuring the level of tonic inhibition in hippocampal slices in eEF2K-KO mice and WT littermates. We chose to carry out electrophysiological recordings in granule cells of the DG, where we had already measured mPSCs, since tonic inhibition is well described in the DG and accounts for approximately 75% of total inhibition in this area (Glykys and Mody 2007). The experimental framework we implemented to analyze tonic inhibition represents a slight modification of a previous design (Farisello et al. 2013) and consists of 3 consecutive phases: GABAergic currents are first measured under relatively physiological conditions, then after stimulation with exogenous GABA, and lastly after blocking $GABA_AR$ currents with the $GABA_AR$ antagonist bicuculline. Kinurenic acid (KYN) was added in all conditions as a broad-spectrum excitatory amino acid antagonist. eEF2K-KO mice showed a marked increase in tonic inhibition relative to WT littermates (Fig. 2A). Antagonizing GABA transporters with NO-711 (data not shown) has no genotype-specific effects, altogether indicating an increased efficacy of extrasynaptic $GABA_ARs$ in the KO mice. To further confirm these results, we used the unspecific $GABA_AR$ agonist muscimol instead of GABA. Again, we found a strong increase in tonic inhibition, which strongly argues for a participation of $GABA_ARs$ in mediating the increased tonic inhibition in eEF2K-KO mice (Fig. 2B). Since in granule cells tonic inhibition is mainly mediated by extrasynaptically located populations of $GABA_ARs$ containing either the δ or α5 subunit (Scimemi et al. 2005; Glykys and Mody 2007), we were interested in deciphering which specific population of receptors mediates the increase in tonic inhibition in eEF2K-KO mice. No difference between the groups was found when the δ-specific agonist 4,5,6,7-tetrahydroisoxazolo[5,4-c]pyridin-3-ol (THIP) was applied (see Supplementary Fig. 2A). Instead, by applying GABA followed by the α5-$GABA_AR$ selective positive allosteric modulator (Margot Ernst, unpublished results) MP (MP-III-004;(*R*)-methyl 8-ethynyl-6-(2-fluorophenyl)-4-methyl-4*H*-benzo[*f*]imidazo[1,5-*a*][1,4]diazepine-3-carboxylate) (provided by Dr James M Cook and Dr Michael M. Poe, Department of Chemistry and Biochemistry, University of Wisconsin Milwaukee, patent US 20100004226 A1), we observed a stronger tonic inhibition in the eEF2K-KO mice compared with WT littermates (Fig. 2C). Consistently, the application of muscimol followed by a co-application of the α5-subunit specific inverse agonist L-655,708 led to a stronger reduction of tonic inhibition in eEF2K-KO mice as opposed to WT mice (Fig. 2D) but no change in phasic currents (data not shown). However, tonic inhibition under baseline conditions (control vs. Bicuculline + KYN) did not differ between eEF2K-KO mice and their littermates (Fig. 2A), indicating that eEF2K activity negatively regulates tonic inhibition in vivo primarily when network activity is strongly increased and levels and GABA diffusion can lead to a strong activation of extrasynaptic $GABA_ARs$ (Scimemi et al. 2005; Farisello et al. 2013).

Next, we examined whether genetic deletion of eEF2K has other visible effects on GABAergic transmission in vivo. For this, we analyzed the dominant frequency of β/γ oscillations induced by kainate application to the CA3 region of the hippocampus. β/γ (20–80 Hz) oscillatory activity in the CA3 subregion is thought to be involved in the encoding and retrieval of information (Treviño et al. 2007; Pietersen et al. 2009) and the frequency of β/γ oscillations in the CA3 subregion is regulated by GABAergic interneurons. Kainate, an agonist for AMPA/kainate receptors, is able to evoke persistent β/γ oscillations, probably through the excitation of interneurons leading to a massive increase of tonic GABA-mediated inhibition on principal cells (Ben-Ari and Cossart 2000).

The power of kainate-induced β/γ oscillations gradually increased during the first 30 min of incubation with the drug and then remained stable for another 45 min (Fig. 2E; see Supplementary Fig. 2B,C). Peak power values did not differ significantly in slices from mutant and WT animals. However, there was an overall significant genotype-specific effect on the dominant frequency of kainate-induced β/γ oscillations after 60 and 75 min of incubation with kainite since hippocampal slices derived from eEF2K-KO showed a higher frequency of β/γ oscillations compared with WT mice (Fig. 2F), suggesting that GABAergic activity is increased in the eEF2K-KO mice following the increased activity of the network.

Taken together, our data show that eEF2K-KO mice exhibit normal excitatory synaptic transmission while inhibitory synaptic transmission is clearly increased. This, in combination with the fact that eEF2K activity in vitro strongly depresses inhibitory synaptic transmission indicates that eEF2K activity modulates the excitation/inhibition balance.

eEF2K Activity Regulates the Expression of a Subset of Synaptic Proteins

To explore which synaptic proteins are controlled by eEF2K activity and mediate the modulatory activity on the excitation/inhibition balance, we utilized stable isotope labeling in cell culture (SILAC) (Mann 2006), in a condition where the isotope integration in the proteome was successful at about 95% (see Supplementary Fig. 3A). We compared infected primary cultures of rat hippocampal neurons at DIV 1 with lentiviruses for the overexpression of either a constitutively active form of eEF2K (eEF2Kca) (Verpelli et al. 2010) or GFP and verified by western blotting (WB) that eEF2K and peEF2 levels were increased by eEF2Kca overexpression (see Supplementary Fig. 3B). We also analyzed Caspase-3 cleavage as an indication of cell viability/apoptosis and could not detect differences between the groups (see Supplementary Fig. 3C). At DIV 20, (crude) synaptosomal P2 fractions were prepared and analyzed by mass spectrometry to identify proteomic differences (see Supplementary Fig. 3D). The SILAC-based mass spectrometry analysis was carried out on 3 independent experiments, each yielding about 1100 identified proteins in the P2 fractions.

By applying stringent parameters (view materials and methods), the analysis revealed 3 proteins (TRIM3, MAP1b, and eEF2) that were upregulated in eEF2Kca and 3 proteins (Synapsin2, CASK, and Glypican-4) that were downregulated (see Supplementary Table 1).

These results were confirmed through western blotting analysis, using the same experimental framework (infection at DIV 1, analysis at DIV 20) without SILAC labeling (Fig. 3A,B). We found that Syn2b (and not Syn2a) levels were significantly and selectively decreased in eEF2Kca-expressing neurons (Fig. 3A,B). The expression of many other presynaptic and postsynaptic proteins was not modified in eEF2Kca-expressing neurons (see

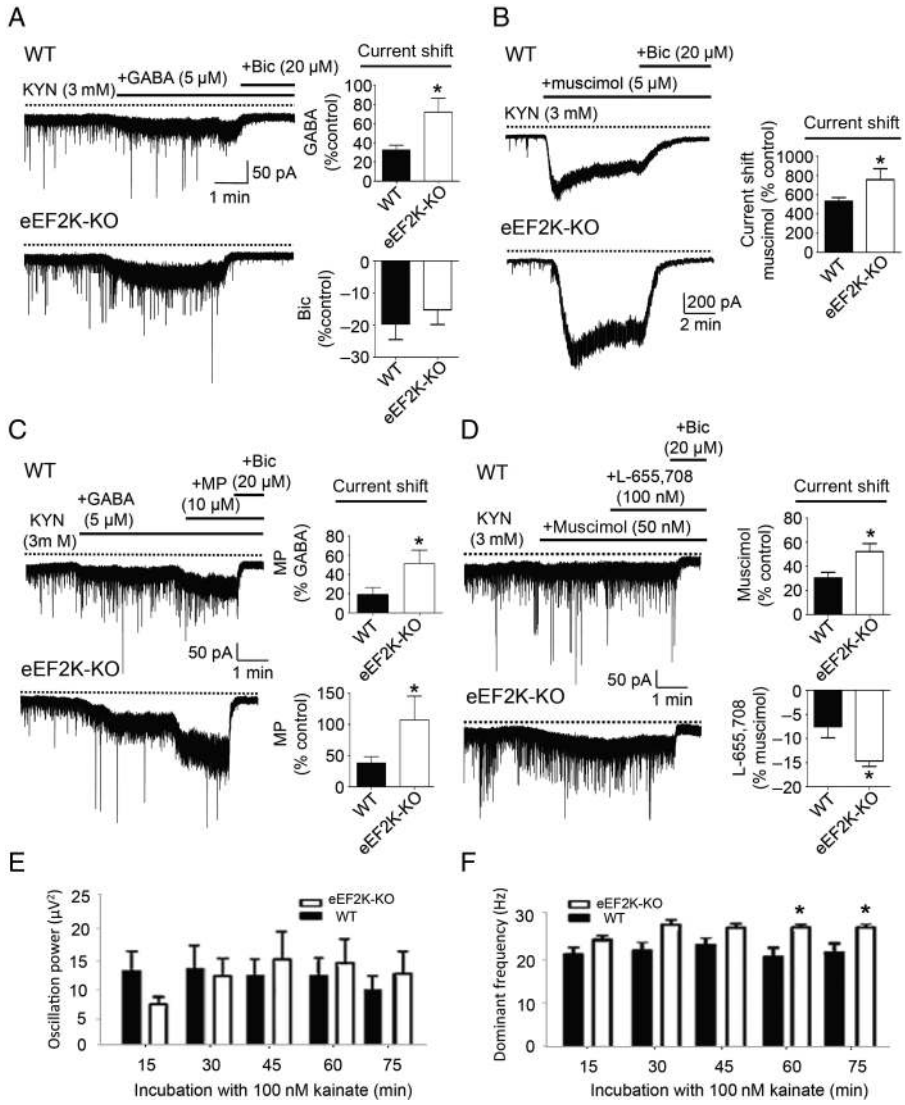

Figure 2. eEF2K-KO mice exhibit increased $GABA_AR\alpha5$-mediated tonic inhibition and a higher frequency of kainite-induced β/γ oscillations. (*A*) Representative current traces of granule cells (hippocampal slices) recorded in voltage-clamp mode (holding potential −65 mV) from WT and eEF2K-KO mice in the presence of Kinurenic acid (KYN) before and after application of exogenous GABA and after application of bicuculline (Bic). Zero current is indicated by dotted line. eEF2K-KO mice (P28–42) show stronger tonic GABAergic currents after GABA application than WT mice. The graph shows the quantification of GABAergic tonic currents of WT and eEF2K-KO mice. An analysis of the current shift is shown (GABA and Bic vs. control). Error bars are SEMs. $N = 22–24$ neurons from at least 8 different animals per group. *$P < 0.05$ versus WT (Student's *t*-test). (*B*) Representative current traces of granule cells (hippocampal slices) recorded in voltage-clamp mode (holding potential −65 mV) from WT and eEF2K-KO mice in the presence of KYN before and after application of muscimol, and after application of Bic. Zero current is indicated by a dotted line. eEF2K-KO mice show stronger tonic GABAergic currents after muscimol application than WT mice. Mice were analyzed at P28–42. The graph shows the quantification of GABAergic tonic currents of WT and eEF2K-KO mice. An analysis of the current shift is shown (muscimol vs. control). Error bars are SEMs. $N = 9–15$ neurons from 4 different animals per group. *$P < 0.05$ versus WT (Student's *t*-test). (*C*) Representative current traces of granule cells (hippocampal slices) recorded in voltage-clamp mode (holding potential −65 mV) from WT and eEF2K-KO mice in the presence of KYN before and after application of exogenous GABA, after coapplication of exogenous GABA and MP-III-004 (SH-053-2′F-R-CH3 methyl ester), and after application of Bic. Zero current is indicated by dotted line. eEF2K-KO mice (P28–42) show stronger tonic GABAergic currents after exogenous GABA application and exhibit even stronger currents after coapplication of MP as opposed to WT mice. The graph shows the quantification of GABAergic tonic currents of WT and eEF2K-KO mice. An analysis of current shift is shown (GABA + MP-III-004 vs. control, as well as GABA + MP-III-004 vs. GABA). Error bars are SEMs. $N = 7–9$ neurons from 3 different animals per group. *$P < 0.05$ versus WT (Student's *t*-test). (*D*) Representative current traces of granule cells (hippocampal slices) recorded in voltage-clamp mode (holding potential −65 mV) from WT and eEF2K-KO mice in the presence of KYN before and after application of muscimol, after coapplication of muscimol and L-655,708, and after application of Bic. Zero current is indicated by dotted line. eEF2K-KO mice (P28–42) show stronger tonic GABAergic currents after muscimol application and also exhibit a stronger reduction in currents after application of L-655,708 as opposed to WT mice. The graph shows the quantification of GABAergic tonic currents of WT and eEF2K-KO mice. An analysis of current shift is shown (muscimol vs. control, as well as muscimol + L-655,708 vs. muscimol). Error bars are SEMs. $N = 9–10$ neurons from 4 different animals per group. *$P < 0.05$ versus WT (Student's *t*-test). (*E*) Time course of β/γ oscillation power upon incubation with 100 nM kainate. Increased β/γ oscillation power as a function of the incubation time with 100 nM kainate in eEF2K-KO mice. eEF2K-KO mice ($n = 20$, $N = 8$), WT ($n = 13$, $N = 7$). Nonsignificant increase of β/γ oscillation power upon incubation with 100 nM kainate was observed. Two-way nested ANOVA, $P > 0.05$. (*F*) An overall significant genotype effect on the dominant frequency of kainate-induced β/γ oscillations was observed. Data are expressed as mean ± SEM. Statistical significance of differences of mean values between the 2 genotypes was determined by post hoc Bonferroni tests showing that values of dominant oscillation frequencies were significantly higher (*$P < 0.05$) after 60 and 75 min of incubation with kainate in slices from eEF2K-KO animals ($n = 20$, $N = 8$) compared with their WT littermates ($n = 13$, $N = 7$).

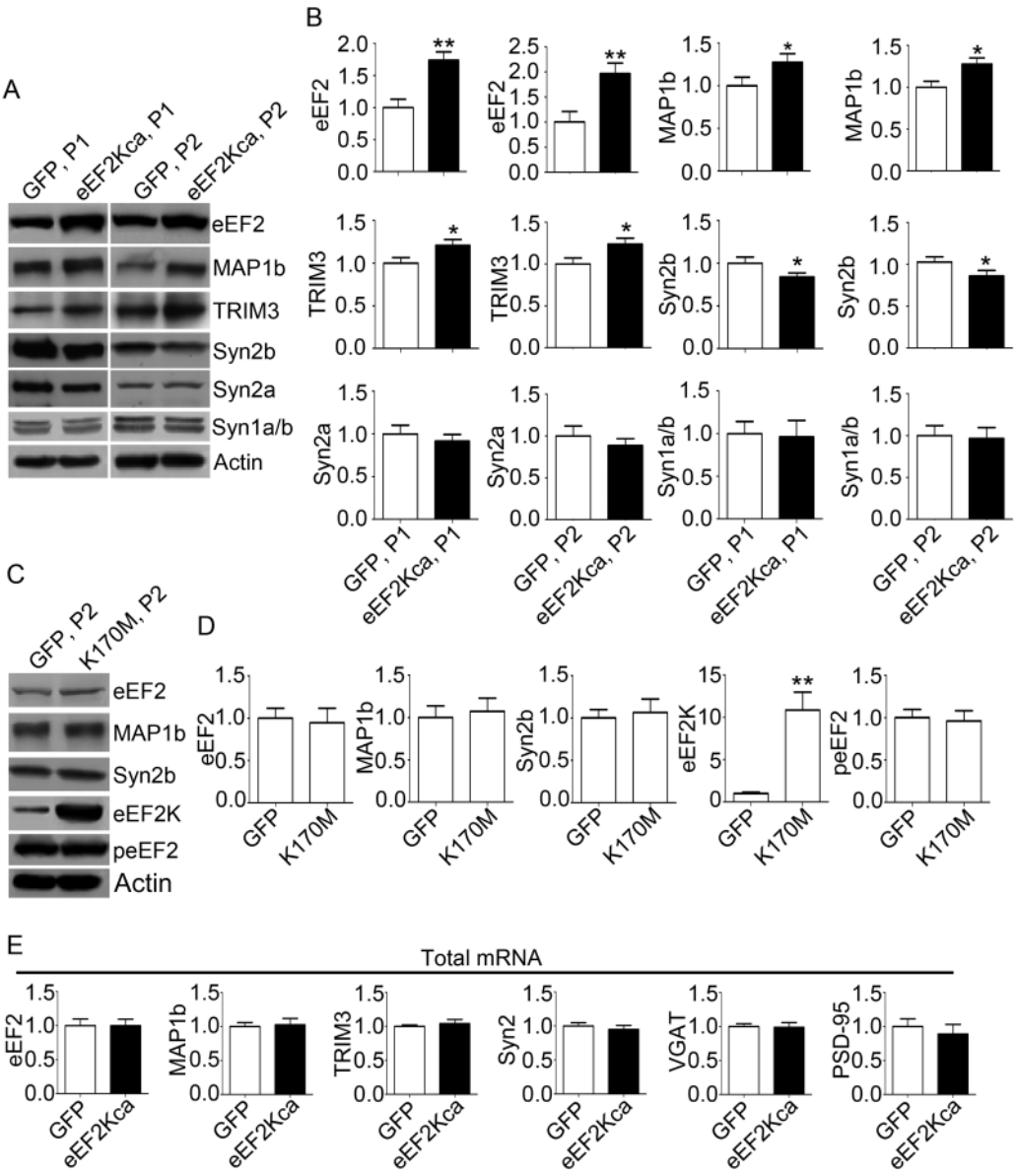

Figure 3. eEF2K activity regulates the expression levels of a set of synaptic proteins. (*A*) Representative WBs showing expression levels of selected eEF2K-regulated synaptic proteins. Primary rat neuronal cultures were infected at DIV 1 with lentiviruses mediating GFP or eEF2Kca overexpression. At DIV 20, nuclear fractions (P1) and crude synaptosomal fractions (P2) were analyzed by WB for eEF2, MAP1b, TRIM3, Syn2b, Syn2a, and Syn1a/b. (*B*) Quantification of relative expression level of selected eEF2K-regulated synaptic proteins. Vertical axis shows the mean fold change in eEF2K over GFP-expressing neurons. Error bars are SEMs. $N \geq 5$ samples from cell cultures derived from different animals. $^{*}P < 0.05$, $^{**}P < 0.01$ versus GFP (Student's *t*-test). (*C*) Representative WBs showing expression levels of selected eEF2K-regulated synaptic proteins in neurons expressing K170 M kinase-dead eEF2K. Primary rat neuronal cultures were infected at DIV 1 with lentiviruses mediating GFP or K170 M overexpression. At DIV 20, crude synaptosomal fractions (P2) were analyzed by WB for eEF2, MAP1b, Syn2b, eEF2K, and peEF2. (*D*) Quantification of the results shown in *D*. Vertical axis shows the mean fold change in K170 M over GFP overexpressing neurons. Error bars are SEMs. $N \geq 5$ samples from cell cultures derived from different animals. $^{**}P < 0.001$ versus GFP (Student's *t*-test). (*E*) Quantitative RT–PCR analysis of selected eEF2K-regulated synaptic proteins. Primary rat neuronal cultures were infected at DIV 1 with lentiviruses mediating GFP or eEF2Kca overexpression. At DIV 20, lysates were analyzed by quantitative RT–PCR for selected eEF2K-regulated proteins (eEF2, MAP1, and Syn2). mRNA levels were standardized by GAPDH expression. Vertical axis shows the mean fold change in eEF2K over GFP-expressing neurons. The analysis reveals that eEF2K does not regulate identified proteins at the level of transcription. Error bars are SEMs. $N = 3$ samples from cell cultures derived from different animals.

Supplementary Fig. 4*A*,*B*). We then generated a lentivirus expressing a previously described (Pyr Dit Ruys et al. 2012), catalytically inactive form of eEF2K (K170 M), and analyzed eEF2, MAP1b, and Syn2b expression. We found that both MAP1b and eEF2 up- and Syn2b downregulation do not take place in K170 M (Fig. 3*C*,*D*), suggesting that in cultured neurons the catalytic activity of eEF2K and the phosphorylation of eEF2 are required for eEF2K-dependent protein expression control to take place.

We also analyzed the relative mRNA levels by quantitative real-time PCR and found no difference between GFP and eEF2Kca overexpressing samples, suggesting that the proteins are not regulated at the transcriptional level (Fig. 3*E*).

To understand whether the identified proteins are linked to the potentiated GABAergic synapse in the eEF2K-KO mice, we used neuronal cultures from eEF2K-KO and WT mice in which we can easily modulate the expression of eEF2K by reintroducing

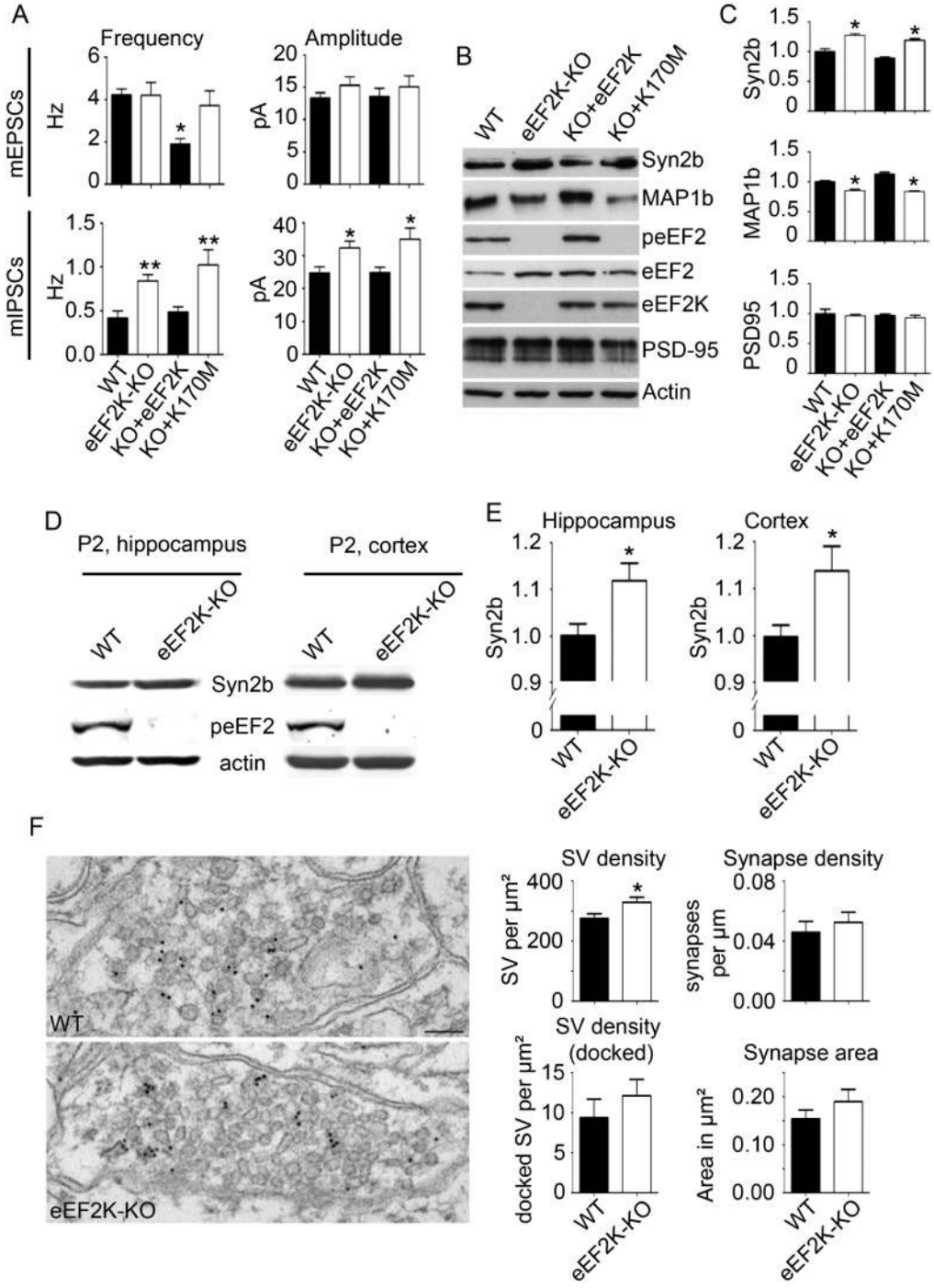

Figure 4. The eEF2K/eEF2 pathway regulates Syn2b expression. (*A*) Quantification of mPSC parameters of WT, eEF2K-KO, and eEF2K-KO primary neuronal cultures infected with a lentivirus expressing eEF2K or K170 M. Error bars are SEMs. *N* = 15 neurons from at least 3 cell cultures derived from different animals. * and **$P < 0.05$ and 0.01 versus WT and KO + eEF2Kca (ANOVA and post hoc Tukey test). (*B*) Primary neuronal mouse cultures from eEF2K-KO mice were infected at DIV 1 with eEF2Kca or K170M-mediating lentiviruses. At DIV 20, lysates were analyzed via WB for the proteins indicated on the right side of the panel. Representative WBs for cultures of WT, eEF2K-KO, and eEF2K-KO infected with a lentivirus expressing eEF2K, eEF2K-KO infected with a lentivirus expressing eEF2K-K170 M. (*C*) The graph shows the quantifications of Syn2b, MAP1b, and PSD-95 in WBs from neurons mouse cultures of WT, eEF2K-KO, and eEF2K-KO infected with a lentivirus expressing eEF2K, eEF2K-KO infected with a lentivirus expressing eEF2K-K170 M. Vertical axis shows the mean fold change WT, eEF2K-KO, eEF2K-KO plus eEF2K, and eEF2K-KO plus eEF2K-K170 M. Error bars are SEMs. *N* = 7/10 samples from at least 3 cell cultures derived from different animals. *$P < 0.001$ versus WT and eEF2K-KO plus eEF2Kca (ANOVA and post hoc Tukey test). (*D*) Representative WBs of P2 fractions from WT and eEF2K-KO mice. The analysis reveals abolished peEF2 and increased Syn2b expression levels in eEF2K-KO mice. P2 fractions of eEF2K-KO and WT mice (P28–P42 for hippocampal slices, P28–P120 for cortex) were prepared from brain slices containing the hippocampus (left) or from cortical brain homogenates (right). (*E*) P2 fractions were analyzed for Syn2b expression and eEF2 phosphorylation (peEF2) by WB. The graph shows the quantification of the relative expression of Syn2b in P2 fractions of WT and eEF2K-KO mice. Vertical axis shows the mean fold change of eEF2K-KO versus WT mice. Error bars are SEMs. *N* = 7/15 samples from different mice per group for hippocampal slices/cortical brain homogenates. *$P < 0.05$ versus WT (single sample *t*-test). (*F*) Representative TEM images of inhibitory synapses in WT and eEF2K-KO mice in the molecular layer of the dentate gyrus. Inhibitory synapses were verified by staining the samples with anti GABA antibodies and colloidal gold-conjugated secondary antibodies. Scale bar, 100 nm. The graphs show morphometric

the kinase via a lentivirus vector. We first performed an electrophysiological analysis in the cultures evaluating synaptic transmission. Interestingly, we observed a strong increase in mIPSC frequency and amplitude in eEF2K-KO mice (Fig. 4A; see Supplementary Fig. 5A–C), while the mEPSC were not different in any parameters compared with WT mice (Fig. 4A; see Supplementary Fig. 5A–C). In the eEF2K-KO neuronal cultures, the reintroduction/expression of eEF2K, but not the expression of the catalytically inactive mutant K170 M, was sufficient to restore most of the mIPSC parameters to the WT cultures, aside from the frequency of mEPSC that was reduced by the expression of eEF2K in the eEF2K-KO cultures. Thus, the analysis in eEF2K-KO neuronal cultures further indicates that the genetic deletion of eEF2K is associated with a higher efficacy of GABAergic synapses.

We then used the cultures to correlate the change of the synaptic properties with the altered protein expression identified by the proteomic analysis. Because eEF2K inhibits general mRNA translation by phosphorylating eEF2, we first looked at the general changes in protein translation using the SUnSET method (Schmidt et al. 2009; Hoeffer et al. 2011). However, we were not able to see a significant increase of general protein synthesis in the neuronal cultures from eEF2K-KO mice compared with WT mice (see Supplementary Fig. 6), indicating that the eEF2K/eEF2 pathway in neurons probably regulates the translation of a subset of mRNAs as suggested by our proteomic data. We then used WB analysis and found that in cultured neurons from eEF2K-KO mice the expression of Syn2b was higher, while MAP1b was lower compared with WT. This differential expression was restored to WT levels in the eEF2K-KO cultured neurons by the reintroduction of active eEF2K (but not the inactive mutant K170 M) (Fig. 4B,C). We were not able to see any change in the expression of eEF2 (Fig. 4B,C) and TRIM3 (data not shown) in the eEF2K-KO cultures.

We then looked at biochemical changes in the eEF2K-KO mice and focused our attention on the 2 proteins that were regulated by eEF2K activity in vitro in neuronal cultures, MAP1b and Syn2b. We analyzed cortical P2 fractions from brain homogenates and P2 fractions obtained from brain slices containing the hippocampus by western blot using a quantitative fluorochrome-based detection system since we expected small proteomic changes in vivo, given the capabilities of mammals to exhibit genetic buffering (Bourgeron 2015). Importantly, a small but replicable ($n = 15$ mice) and significant upregulation of Syn2b levels was observed (Fig. 4D,E). The analysis of MAP1b levels revealed no difference between eEF2K-KO mice and their WT littermates (data not shown). These results further indicate that the eEF2K/eEF2 pathway regulates Syn2b expression levels both in vitro and in vivo. Using fluorochrome-based WB, we also looked at the expression of the α5-containing $GABA_A$ receptor (which was not identified in the proteomic analysis, that is, the mass spectrometry gave no information regarding this molecule) considering that the electrophysiological measurement of increased tonic inhibition seems to be mediated by this receptor. Indeed, eEF2K-KO mice show a small but significant increase in levels of the α5 $GABA_A$ receptor subunit in the hippocampus, while the α1 $GABA_A$ subunit only showed a slight trend for an increase in the eEF2K-KO mice compared with WT (see Supplementary Fig. 7A,B).

Finally, we performed an ultrastructural analysis of inhibitory synapses of DG granule cells. This analysis revealed an increase in synaptic vesicle density in GABAergic synapses of eEF2K-KO mice compared with WT (Fig. 4F), consistent with an increase in mIPSC frequency. No changes in docked vesicles or synapse area could be observed (Fig. 4F). In line with our electrophysiological results from eEF2K-KO mice, the excitatory synapses' ultrastructural morphology was unchanged compared with WT mice (see Supplementary Fig. 8). Worthy of note, Syn2-KO mice have a decreased vesicle density at inhibitory synapses of hippocampal DG granule cells and exhibit a reduced mIPSC frequency without changes in evoked IPSCs in these cells (Medrihan et al. 2013). Thus, the alterations at the GABAergic presynapse that we observe in eEF2K-KO mice are specular to those of Syn2-KO mice, possibly being related to the increase in Syn2b levels observed in eEF2K-KO mice.

To further prove that the effect of eEF2K activity on synaptic transmission is mediated mainly by the alteration of Syn2b levels, we used 2 different approaches:

We first identified and used specific Syn2b siRNA to knock down the expression of Syn2b (Fig. 5A–C) and occlude the effect of eEF2Kca overexpression. Indeed, both the mEPSC and mIPSC frequencies were reduced in rat neurons with reduced levels of Syn2b and were not further reduced by the coexpression of eEF2K-ca (Fig. 5D; see Supplementary Fig. 9A,B). Interestingly, mIPSC and mEPSC amplitude, decay time, and area were not affected by the siRNA knock down of Syn2b but mIPSC amplitude, decay time, and area were reduced by the coexpression of eEF2Kca (Fig. 5D; see Supplementary Fig. 9A,B).

Finally, with the second approach, we also found that the eEF2K-induced reduction in both mEPSC and mIPSC frequencies (but not mIPSC amplitude, decay time, and area) were rescued by the co-expression of Syn2b (Fig. 5E,F; see Supplementary Fig. 9C,D).

All these data strongly indicate that eEF2K activity regulates synaptic transmission at the presynaptic level by modulating the expression of Syn2b and the efficacy of inhibitory synapses at the postsynaptic site independently of Syn2b modulation.

eEF2K-KO Mice Are Less Prone to Seizures

The above electrophysiological *ex vivo* results suggest that eEF2K-KO mice exhibit an increased tonic inhibition and potentiated mIPSCs in the DG of the hippocampus, which is known to be a source for focal epileptic activity (Toader et al. 2013). We wanted to test whether these mice show a decreased susceptibility to seizures relative to WT littermates when they are challenged with chemoconvulsive substances. Indeed, the GABAergic system and tonic inhibition are causally related to seizures, as in many cases a lower tonic inhibition appears to be one of the root causes of status epilepticus and seizures (Klitgaard 2005; Maguire et al. 2005; Scimemi et al. 2005; Farisello et al. 2013; Pavlov and Walker 2013). Seizures were induced by pentylenetetrazol (PTZ) or pilocarpine in eEF2K-KO and WT mice while carrying out electroencephalographic (EEG) recordings and analysis as previously described (Sala et al. 2011). A subconvulsive dose of PTZ (Jelenković et al. 2002) or a convulsive dose of pilocarpine (Vezzani 2009)

analyses of inhibitory synapses ultrastructure in WT ($N = 3$) and eEF2K-KO ($N = 3$) mice indicate an increase of SV density in inhibitory synapses of eEF2K-KO mice. Error bars are SEMs. Mean values of SV density: 275.8 ± 15.04 in WT ($n = 87$) and 328.8 ± 17.22 vesicle/μm² in eEF2K-KO ($n = 89$). *$P < 0.05$ (nonparametric Welch's *t*-test). The density of docked vesicles is unchanged between WT and eEF2K-KO mice: 9.390 ± 2.302 in WT ($n = 63$) and 12.13 ± 2.02 vesicle/μm² in KO mice ($n = 79$) (2-tailed *t*-test). A docked vesicle is defined as a vesicle with its center located within 20 nm from the presynaptic membrane. The number of inhibitory synapses is unchanged between eEF2K-KO and WT mice: 0.045 ± 0.007 in WT ($n = 40$) and 0.052 ± 0.006 no. of synapses/μm in eEF2K-KO mice ($n = 40$) (2-tailed *t*-test); the number of inhibitory synapses was determined by counting the number of GABAergic synapses per micrometer of neuron soma perimeter measured on images acquired at low magnification. The average cross-sectional synaptic area is 0.1542 ± 0.018 in WT ($n = 63$) and 0.191 ± 0.025 μm² in KO mice ($n = 79$) and is therefore unchanged (2-tailed *t*-test).

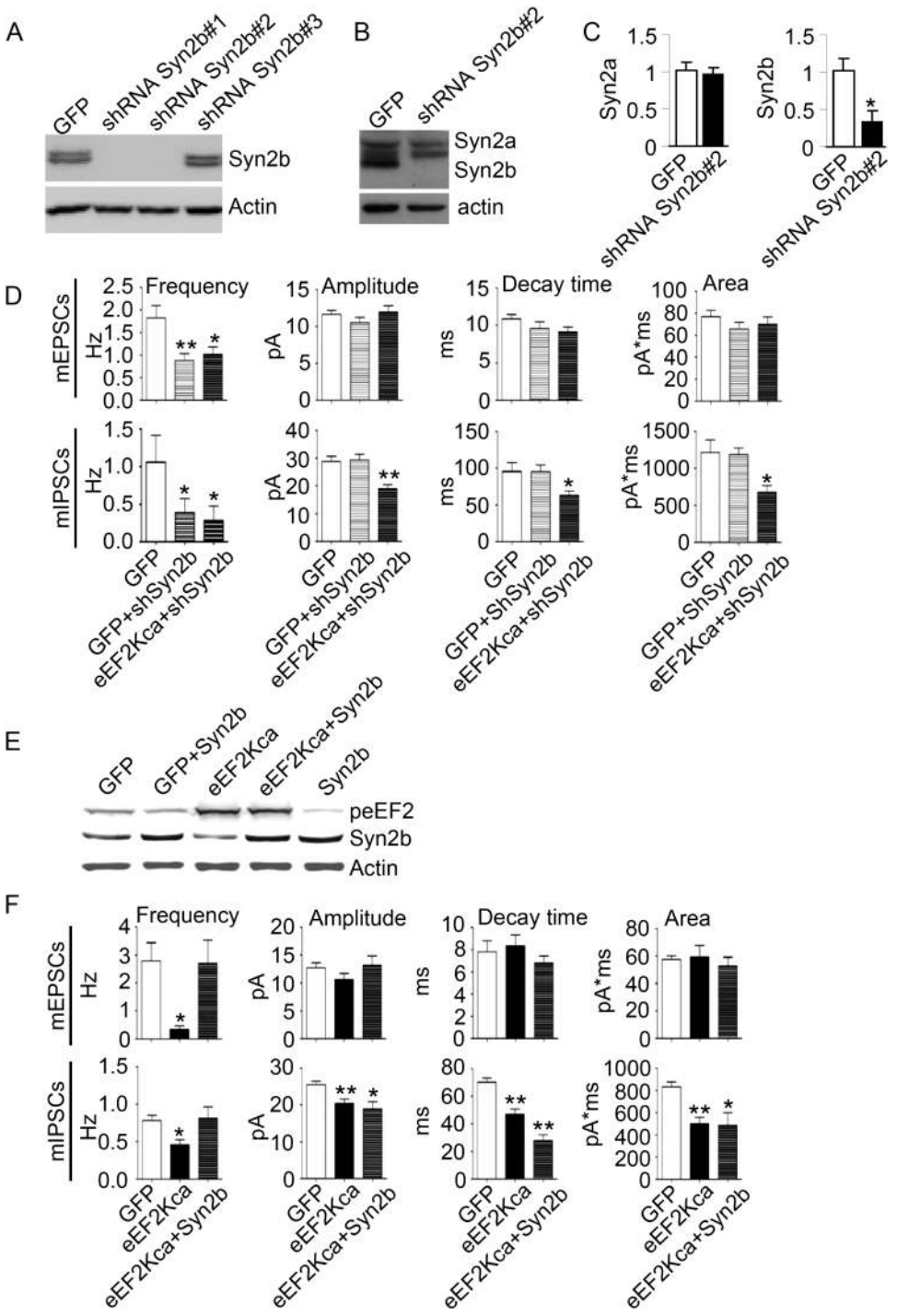

Figure 5. eEF2K activity downregulates mPSC frequency in a Syn-dependent fashion. (*A*) Representative WBs for COS-7 cells transfected with Syn2b plus GFP, Syn2b plus shRNA Syn2b#1, Syn2b plus shRNA Syn2b#2, and Syn2b plus shRNA Syn2b#3. COS-7 cells were lysed and analysed by WB for the expression of Syn2b 48 h after the transfection. Only the shRNA Syn2b#1 and shRNA Syn2b#2 were able to inhibit the expression of Syn2b. (*B*) Representative WBs for GFP and shRNA Syn2b#2 overexpressing neurons. The shRNA Syn2b#2 was able to strongly inhibit the expression of endogenous Syn2b but not Syn2a. Primary neuronal rat cultures were infected at DIV 1 and lysed at DIV20 and analyzed via WB for Syn2a and Syn2b. (*C*) The graphs show the quantifications of Syn2a and Syn2b in WBs. Vertical axis shows the mean fold change GFP versus shRNA Syn2b#2 overexpressing neurons. Error bars are SEMs, $n = 9$ samples from at least 3 cell cultures derived from different animals. *$P < 0.01$ versus GFP (Student's *t*-test). (*D*) Quantification of mPSC parameters of GFP, GFP plus shSyn2b, and eEF2Kca plus shSyn2b overexpressing neurons. Primary neuronal rat cultures were infected at DIV 1 with the described combination of lentiviruses and analyzed at DIV20. Error bars are SEMs. $N = 15$ neurons from at least 3 cell cultures derived from different animals. * and **$P < 0.05$ and 0.01 versus GFP (ANOVA and post hoc Tukey test). (*E*) Representative WBs for GFP, GFP plus Syn2b, eEF2Kca, eEF2Kca plus Syn2b, and Syn2b overexpressing neurons. Primary neuronal rat cultures were infected at DIV 1, lysed at DIV 20, and analyzed via WB for peEF2 and Syn2b. (*F*) Quantification of mPSC parameters of GFP, eEF2Kca, and eEF2Kca plus shSyn2b overexpressing neurons. Primary neuronal rat cultures were infected at DIV 1 with the described combination of lentiviruses and analyzed at DIV20. Error bars are SEMs. $N = 15$ neurons from at least 3 cell cultures derived from different animals. * and **$P < 0.05$ and 0.01 versus GFP (ANOVA and post hoc Tukey test).

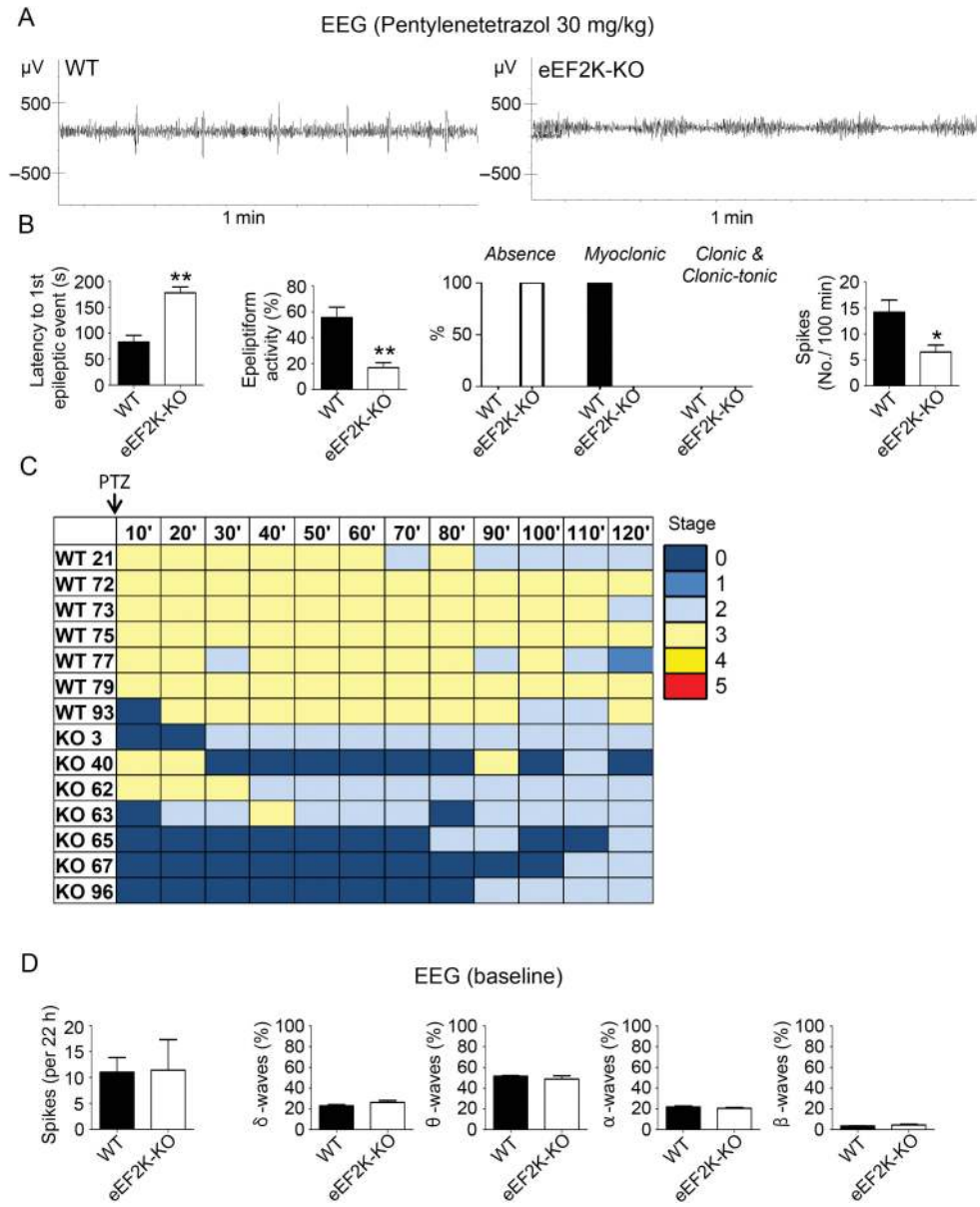

Figure 6. eEF2K-KO mice show a reduced susceptibility to seizures while exhibiting normal baseline brain activity. (*A*) Representative EEG traces after PTZ injection. eEF2K-KO mice are clearly less susceptible to seizures than WT mice. A subconvulsive dose of PTZ (30 mg/kg) was administered to WT and eEF2K-KO (P75–P90), followed by immediate recording of EEG activity. (*B*) Quantifications of several behavioral and EEG parameters after PTZ injection. Vertical axis shows latency to first epileptic event, time spent in epileptiform activity, % of mice exhibiting absence, myoclonic or clonic & clonic–tonic seizures, and number of EEG spikes per 100 min. Error bars are SEMs. $N = 7$ animals per group. * and **$P < 0.05$ and 0.001 versus WT (Student's *t*-test). (*C*) Racine scale analysis (different colors for each stage, see Experimental Procedures) after PTZ injection. Each animal's maximum seizure score was measured every 10 min over a 2-h period following the Racine scale associated with the EEG scale (Jinde et al. 2012). (*D*) EEG analysis of WT and eEF2K-KO mice under basal conditions. WT and eEF2K-KO mice exhibit comparable baseline cortical activity. Basal cerebral activity of WT and eEF2K-KO mice (P75-P90) was recorded continuously for 22 h in freely moving awake mice. Vertical axis shows relative δ, θ, α, and β EEG frequency bands (% of total spectral power) and number of EEG spikes per 22 h. Error bars are SEMs. $N = 11$ animals for EEG frequency band analysis and $n = 7$ animals for EEG spike analysis per group.

was used to measure absence, myoclonic, and clonic/clonic–tonic seizure responses. eEF2K-KO mice exhibited a reduced response in both conditions. After PTZ treatment, eEF2K-KO mice only have absence seizures while wild types exhibit myoclonic seizures (Fig. 6*A–C*), and after pilocarpine treatment, eEF2K-KO mice show a shift toward myoclonic seizures while wild types exhibit clonic and clonic–tonic seizures (see Supplementary Fig. 10*A*,*B*). These results strongly indicate that the absence of eEF2K activity is associated with a decreased susceptibility to seizures. Notably, neither the relative weight of the EEG frequency bands nor the spontaneously occurring EEG spikes differed between eEF2K-KO and WT mice under baseline conditions (Fig. 6*D*; see Supplementary Fig. 10*C* and *D*) suggesting an unaltered basal brain activity in the KO mice, in line with previous work (Gildish et al. 2012). Taken together, these results demonstrate that while the absence of eEF2K activity decreases the susceptibility to seizures, it does not have an effect on brain activity under baseline conditions.

Impaired Hippocampal-Dependent Behavior in eEF2K-KO Mice

Considering the altered balance between excitatory and inhibitory synapses in the eEF2K-KO mice, we tested eEF2K-KO mice in a series of basic or more specific cortex-, hippocampus-, and amygdala-dependent behavioral paradigms. First, we tested differences in novel place of object recognition, locomotion, or emotional responses between the eEF2K-KO mice and their WT littermates. Gross brain architecture, body weight, food intake, body tone, grip strength, clasping, hanging wire, reflexes, and basic sociability were all normal in the eEF2K-KO mice (see Supplementary Fig. 11*A–I*).

To evaluate the ability of eEF2K-KO mice to explore a familiar object in a novel place, a novel place of object recognition test was performed. During this task, mice were allowed to explore 2 objects for 3 days and 24 h following the last learning trial, the mice were tested for recognition of one of the familiar objects in a novel place. eEF2K-KO mice displayed a similar percentage of exploration for the familiar object in a novel place as their WT littermates, suggesting that object recognition ability is normal in eEF2K-KO mice (see Supplementary Fig. 12*A*).

We next tested whether the genetic deletion of eEF2K disrupts basal anxiety-like behavior by performing the open field and elevated plus maze paradigms in the eEF2K-KO mice. In these tests, a decrease in time spent at the center of the open field, a decrease in total distance traveled, or an increase of time spent in the closed arm are commonly used as phenotypic markers of anxiety-like behavior in rodents (Crawley et al. 1997). There was no difference in the time spent at the center of the open field or in the distance covered by eEF2K-KO mice compared with their controls (see Supplementary Fig. 12*B*,*C*). The total number of entries into any arm of the elevated plus maze was comparable in both genotypes, confirming the integrity of motor activity (see Supplementary Fig. 12*D*). In addition, marble burying, another index of anxiety-like behavior, was normal in eEF2K-KO compared with WT mice (see Supplementary Fig. 12*E*). Finally, the measured locomotor activity was also normal in the eEF2K-KO mice (see Supplementary Fig. 12*F*).

Given the absence of basic emotional or motor phenotypes of the eEF2K-KO mice, we tested in detail cortex-, amygdala-, and hippocampus-dependent learning and memory phenotypes. To test cortex-dependent tasks, we performed positive and negative taste learning paradigms (Elkobi et al. 2008; Rosenberg et al. 2014). eEF2K-KO mice displayed normal CTA memory compared with their WT littermates (Fig. 7*A*,*B*). In addition, there was no difference between eEF2K-KO and WT mice regarding novel taste memory since we observed a normal decrease in the neophobic response (see Supplementary Fig. 12*G*). This suggests normal acquisition and processing of taste information in eEF2K-KO mice. Next, we asked whether eEF2K is critical for hippocampal-dependent learning using the MWM, in which the mice use spatial cues to learn the position of a hidden platform (Vorhees and Williams 2006). eEF2K-KO mice were as successful as the control mice in learning the position of hidden platform (Fig. 7*C*). Following the learning period of the MWM task, probe tests were performed 24 h after the last learning trial. Similarly to their WT littermates, eEF2K-KO mice showed a preference for the target quadrant that previously contained the hidden platform (Fig. 7*D*), indicating that eEF2K-KO mice have normal spatial memory. To further elucidate the role of eEF2K in reversal learning of the MWM task, 2 days after the probe test of the standard MWM task the platform location was switched to the opposite quadrant. In this task, cognitive flexibility was assessed, determined by the ability of the mice to learn the new platform position. eEF2K-KO mice exhibited normal reversal learning of MWM compared with WT mice (see Supplementary Fig. 12*H*).

The hippocampus plays a critical role in certain types of associative learning. Pavlovian fear conditioning is widely used as a model to study hippocampus-dependent memory (Segev et al. 2013, 2015). To test hippocampal subregion(s)-dominant roles, we used trace fear-conditioning and delay fear-conditioning paradigms. Trace fear conditioning is similar to delay fear conditioning, except that there is a stimulus-free interval separating the conditioned stimulus (CS) and the unconditioned stimulus (US) presented. Trace fear conditioning depends upon an intact hippocampus (Pierson et al. 2015).

We examined the ability of eEF2K-KO mice to form long-term trace fear conditioning and delay fear conditioning. The paradigms were performed as illustrated in Fig. 7*E*. For trace fear conditioning, animals were subjected to 1 trial of strong trace fear-conditioning protocol in which the tone was separated by 20 s from the shock. Animals were tested 24 h following the conditioning for context and tone tests, and freezing was analyzed during the time window between tone and shock. Interestingly, eEF2K-KO mice exhibited impaired trace fear conditioning compared with WT mice (Fig. 7*F*). In addition, a nonsignificant decrease in freezing was observed in auditory fear conditioning in eEF2K-KO compared with WT mice (Fig. 7*G*), but similar contextual fear conditioning was observed between the different genotypes, indicating that their ability to freeze is normal using a strong protocol (Fig. 7*H*). To better identify hippocampal-dependent learning phenotypes, animals were subjected to 1 trial weak delay fear-conditioning protocol in which the tone was co-terminated with shock. Animals were tested 24 h following the conditioning trial for context and tone tests. Interestingly, eEF2K-KO mice showed impaired contextual fear conditioning compared with WT mice but normal amygdala-dependent auditory fear conditioning (Fig. 7*I*,*J*).

Taken together, the behavioral analysis reveals that eEF2K is essential for the expression of contextual fear memory and DG-dominant trace fear memory, in which, in addition to the context and tone, time processing between CS and US is required (Rodriguez and Levy 2001; Gilmartin and McEchron 2005; Czerniawski et al. 2009; Pierson et al. 2015) and that there is a differential contribution of the eEF2K genetic deletion in the expression of hippocampal-dependent memories.

Given the relatively weak hippocampal-dependent behavioral phenotype of the eEF2K-KO mice, we hypothesized that levels of eEF2 phosphorylation are different in the different subfields of the hippocampus in normal WT mice. Therefore, we preformed immunohistochemistry (IHC) of eEF2 phosphorylation (peEF2) in CA1, CA3, and DG. Indeed, a differential expression pattern of peEF2 but not eEF2 proteins in the hippocampus subregions was observed (see Supplementary Fig. 13*A–C*). Higher levels of peEF2 were observed in the CA3 and DG subregions compared with the CA1 (see Supplementary Fig. 13*C*). As expected, there was no peEF2 in the eEF2K KO mice (see Supplementary Fig. 13*A*).

Genetic and Pharmacological Inhibition of eEF2K Activity Rescues an Epileptic Phenotype in Syn1 KO Mice

Our findings suggest that the eEF2K/eEF2 pathway regulates the excitatory/inhibitory balance in the DG of the hippocampus at the mRNA translation level and that inhibition of this pathway pushes the balance toward the inhibitory side. Since it has previously been demonstrated that Syn1-KO mice have an increased seizure propensity and replicate the epileptic phenotype present

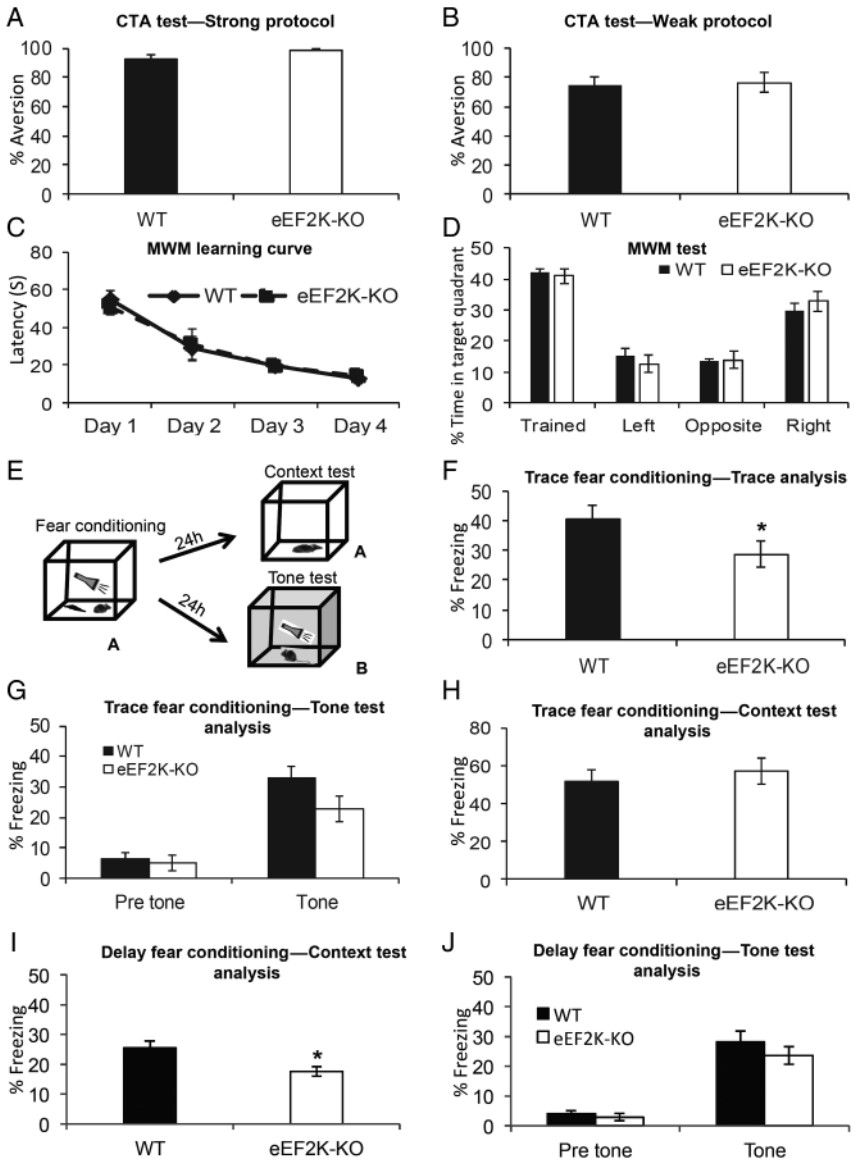

Figure 7. Genetic deletion of eEF2K specifically disrupts contextual and trace fear-conditioning formation. (*A*,*B*) eEF2K-KO mice display normal CTA memory compared with WT animals in both weak (0.075 M LiCl) and strong (0.14 M LiCl) protocols. eEF2K-KO ($n = 9$), WT ($n = 13$) for both protocols. Error bars are SEMs. Student's *t*-test; $P > 0.05$. (*C*) eEF2K-KO mice display normal Morris water maze (MWM) learning. Escape latency was measured across 4 days of MWM task and shows that eEF2K-KO mice acquired the spatial learning same as control animals. eEF2K-KO ($n = 5$), WT ($n = 7$). Error bars are SEMs. Repeated-measures ANOVA, $P > 0.05$. (*D*) eEF2K-KO mice show normal spatial memory in Morris water maze probe test. Mice were trained using a standard Morris water maze paradigm and tested for spatial memory of platform location in the probe test. Results are displayed as percentage of time spent in each quadrant during the probe test. eEF2K-KO ($n = 5$), WT ($n = 7$). Error bars are SEMs. Student's *t*-test; $P > 0.05$. (*E*) Fear conditioning behavior procedure. Mice received 7 combinations of [tone interval shock] in context *A* using strong trace fear-conditioning protocol. For weak delay fear-conditioning protocol, mice received 1 trial composed of 2 pairings of tone shock in context *A*. Tests were done 24 h following conditioning. Context test was performed in context *A*, and the tone test was performed in context *B*. (*F*) Trace fear conditioning is impaired in eEF2K-KO compared with WT mice. Mice were exposed to the same trial of the conditioning but without shock in a novel context. Freezing, considered as "trace fear conditioning," was measured during the time window between consecutive tones. Average of the first 4 traces is presented and analyzed, as they were less likely to be affected by extinction. eEF2K-KO ($n = 8$), WT ($n = 8$). Error bars are SEMs. Repeated-measures ANOVA, $P < 0.05$. (*G*) Long-term auditory fear conditioning is normal in eEF2K-KO mice using trace fear-conditioning protocol. Mice were exposed to the same tone that was delivered in the conditioning trial in a novel context. Seven presentations of the tone were given as the conditioning trial, 20 s each. Percentage of freezing was calculated during the tone presentation and average of the first 4 tone periods is presented and analyzed, as they less likely to be affected by extinction. eEF2K-KO ($n = 8$), WT ($n = 8$). Error bars are SEMs. Repeated-measures ANOVA, $P > 0.05$. (*H*) Long-term contextual fear conditioning is normal in eEF2K-KO mice using trace fear-conditioning protocol. On the contextual fear-conditioning test, animals were returned to the same chamber of training 24 h after training for 300 s without tone. Long-term contextual fear memory was measured as percentage of time spent freezing during the test trial. eEF2K-KO ($n = 8$), WT ($n = 8$). Error bars are SEMs. Student's *t*-test; $P > 0.05$. (*I*) Long-term contextual fear conditioning is impaired in eEF2K-KO mice using delay fear-conditioning protocol. On the contextual fear-conditioning test, animals were returned to the same chamber of training 24 h after training for 300 s without tone. Long-term contextual fear memory was measured as percentage of time spent freezing during the test trial. eEF2K-KO ($n = 11$), WT ($n = 10$). Error bars are SEMs. Student's *t*-test; $P < 0.05$. (*J*) Long-term auditory fear conditioning is normal in eEF2K-KO mice using delay fear-conditioning protocol. Mice were exposed to the same tone that was delivered in the conditioning trial in a novel context. Three presentations of the tone were given as the conditioning trial, 20 s each. Percentage of freezing was calculated during the tone presentation, and average of the tone periods is presented and analyzed. eEF2K-KO ($n = 11$), WT ($n = 10$). Error bars are SEMs. Repeated-measures ANOVA, $P > 0.05$.

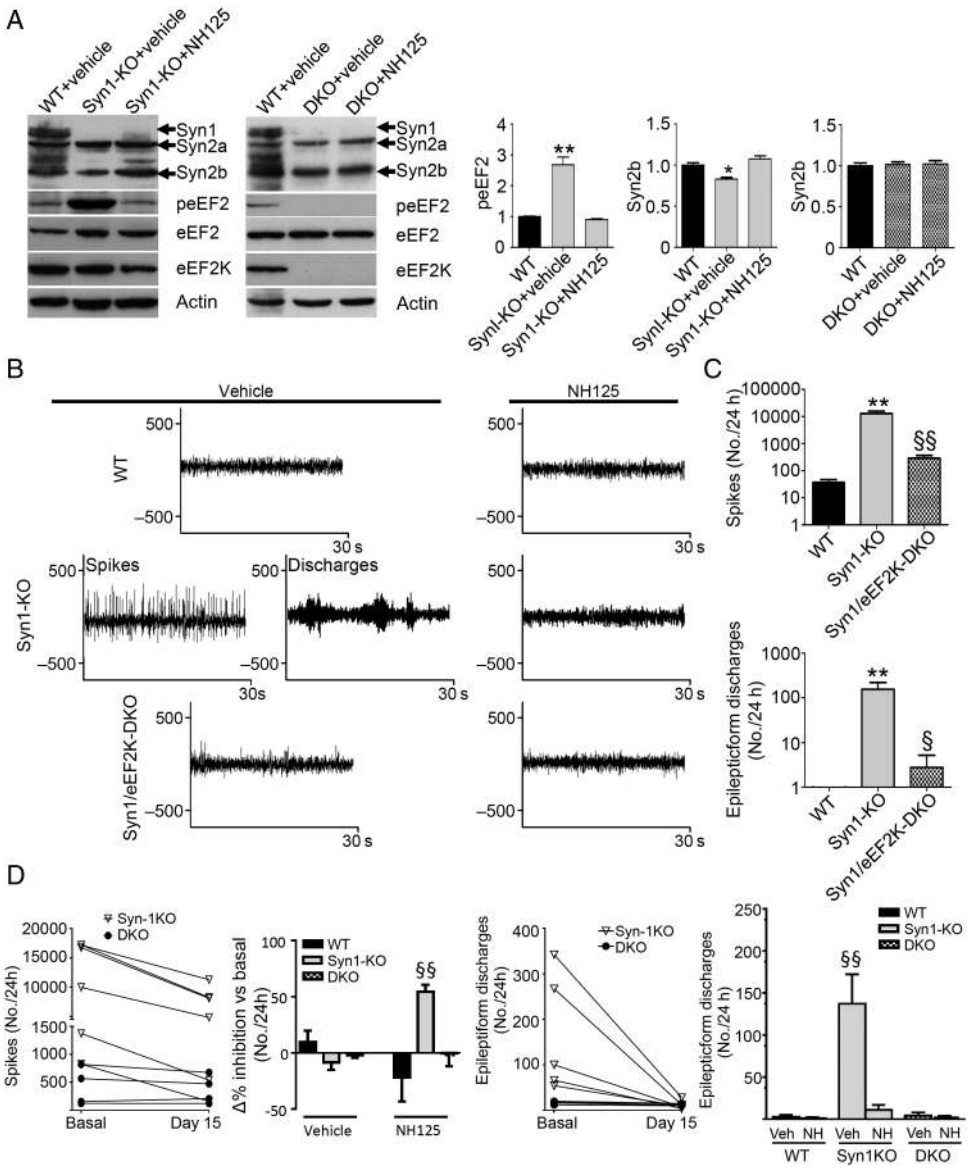

Figure 8. Genetic and pharmacological inhibition of eEF2K activity rescues the epileptic phenotype in Syn1 KO mice. (*A*) Representative WB of P2 fractions obtained from forebrain of WT mice treated with vehicle, Syn1-KO mice, and eEF2K/Syn1 double KO mice treated with vehicle or NH125 (1 mg/kg/day via ip). Syn1 KO mice express high level of peEF2, genetic and pharmacological inhibition of eEF2K activity rescues epileptic phenotype in Syn1 KO mice. The analysis reveals abolished peEF2 and increased Syn2b expression levels in eEF2K-KO mice. P2 fractions of treated and untreated mice at P60 were prepared from isolated hippocampi. The graphs show the quantification of the relative expression of peEF2, Syn2b, and eEF2K in P2 fractions of WT mice treated with vehicle and Syn1 KO mice and eEF2K/Syn1 double KO mice treated with vehicle or NH125. Vertical axis shows the mean fold change of WT mice treated with vehicle versus Syn1 KO mice treated with vehicle or NH125. Error bars are SEMs. $N = 3/5$ samples from different mice per group, * and ** $P < 0.05$ and 0.01 versus WT and Syn1-KO + NH125 (ANOVA and post hoc Tukey test). (*B*) Representative EEG traces (30 s registration is shown) of a WT, Syn1-KO, and eEF2K/Syn1-DKO mouse after vehicle (left) or NH125 (1 mg/kg/day via ip) (right) given for 15 days. For the Syn1-KO mouse, an example of a tracing at high frequency of spikes and a tracing of epileptiform discharges, which can be easily collected during the 24 h recording, are shown. (*C*) Total number of spikes (upper graph) and corresponding epileptiform discharges (lower graph) under basal conditions evaluated for 24 h in freely moving awake WT, Syn1KO, and DKO mice. ** $P < 0.001$ versus corresponding WT; $^{\S}P < 0.01$, $^{\S\S}P < 0.0001$ versus Syn1KO (Tukey's test). (*D*) Effect of vehicle or NH125 treatment on spike activity and epileptiform discharges numbers, evaluated for 24 h before (basal) and after NH125 treatment for the Syn1 KO and eEF2K/Syn1-DKO individual mice; only the Syn1 KO mice showed a clear reduction of the number of spikes and epileptiform discharges after NH125 treatment. NH125 also showed an effect on Δ% of inhibition of both spike activity and epileptiform discharges numbers versus basal (before vehicle or NH125 treatment) during 24 h recording. $^{\S\S}P < 0.001$ versus all the remaining groups. Data are mean ± SEM (where applicable) of 5–7 subjects per group (Student's *t*-test or Bonferroni's test).

in patients with *SYN1* mutations (Li et al. 1995; Gitler et al. 2004; Cambiaghi et al. 2013), we crossed these mice with eEF2K-KO mice to possibly rescue the seizure phenotype. We also investigated whether eEF2K inhibition with NH125, a well-described eEF2K inhibitor (Autry et al. 2011), could be effective in vivo and could revert the epileptic phenotypes in Syn1-KO mice.

Interestingly, we found that the levels of phosphorylated eEF2 was almost 3 times higher in Syn1-KO brains compared with WT and were virtually normalized to WT levels by NH125 treatment (Fig. 8A). In parallel, the expression levels of Syn2b, which was reported to be reduced in Syn1-KO mice (Rosahl et al. 1995), was significantly restored after NH125 treatment (Fig. 8A). In contrast, the expression level of Syn2b in Syn1-eEF2K-double KO mice (Syn1/eEF2K-DKO) was similar to those of WT mice and not modified by treatment with NH125 (Fig. 8A). These data indicate that the eEF2K/eEF2 pathway is dysregulated in SynI KO mice and

that this molecular alteration might markedly contribute to the epileptic phenotype.

Next, the EEG of male WT, Syn1-KO, and Syn1/eEF2K-DKO mice was recorded under basal conditions for 24 h. We found that while Syn1-KO mice displayed an average of 12 645 ± 4156 spikes/24 h (mean ± SE; 8 mice) and WT mice (15 mice), only 36 ± 15 spikes/24 h, Syn1/eEF2K-DKO mice showed 290 ± 95 spikes/24 h (7 mice) (Fig. 8*B*,*C*). Consistently, Syn1-KO mice showed a mean of 156 ± 75 epileptic discharges/24 h compared with only 2.5 ± 2.0 observed in Syn1/eEF2K-DKO (Fig. 8*B*,*C*). Our data indicate that, indeed, the absence of eEF2K has a protective function in the Syn1-KO mouse model of genetic epilepsy. Additionally, we treated WT, Syn1-KO, and Syn1/eEF2K-DKO mice with a daily dose of 1 mg/kg NH125 for 2 weeks and then measured the EEG activity under basal conditions. Strikingly, we found that NH125 reduced the number of spikes to about 45% and virtually eliminated epileptic discharges in Syn1-KO mice, while it was unable, as expected, to reduce the number of spikes in Syn1/eEF2K-DKO mice (Fig. 8*D*).

Discussion

Our study identifies eEF2K as an effective modulator of GABAergic synaptic transmission and points toward practical applications of eEF2K inhibitors in the context of seizure and epilepsy control. Using an eEF2K gain-of-function design in vitro as well as eEF2K-KO mice, we show that eEF2K activity regulates the excitation/inhibition balance by downregulating vesicle release at inhibitory synapses and tonic inhibition. This translates into a reduced susceptibility of eEF2K-KO mice for seizures without major behavioral alterations with the exception of impaired contextual and trace fear memory. In addition, the genetic or pharmacological inhibition of eEF2K can rescue the epileptic phenotype in Syn1 KO mice, a genetic model of human epilepsy. Thus, we propose that chronic administration of eEF2K inhibitors may be an approach to control seizures in patients suffering from this condition.

The eEF2K/eEF2 Pathway Regulates a Subset of Proteins That Modulate Efficacy of GABAergic Synapses

Our findings indicate that eEF2K activity downregulates the function of the inhibitory but not of the excitatory synapses. More specifically, in neuronal cultures, the overexpression of a constitutively active from of eEF2K downregulates the efficacy of both the pre- and postsynaptic compartment of inhibitory synapses and the efficacy of the excitatory synapse only at the presynaptic level. Accordingly, granule cells of dentate gyrus and neuronal cultures from eEF2K-KO mice exhibit potentiated mIPSCs (both pre- and postsynaptically) but normal mEPSCs. Thus, neurons from eEF2K-KO mice do not show alterations in excitatory signal transmission, either pre- or postsynaptically, which one may not have expected based on the aforementioned overexpression in vitro data where an effect on the presynaptic compartment of the excitatory synapse was observed. A possible explanation is that neuronal circuits may have different modalities of compensating a genetic loss of function of a protein as opposed to a situation in which there is an acute gain-of-function of the protein.

Using an unbiased proteomic approach, we then found that eEF2K gain of function in primary neuronal cultures modulates the expression of a subset of synaptic proteins: eEF2K activity reduces the expression of Synapsin2b while increasing the expression of MAP1b as previously demonstrated by Davidkova and Carroll (2007), TRIM3, and eEF2. As expected, mRNA expression of these proteins is not altered indicating that the eEF2K/eEF2 pathway acts at the translational level. These data coincide with observations that eEF2K can specifically regulate a subset of proteins like MAP1B or Arc though the mechanisms of this translational regulation are not clear (Davidkova and Carroll 2007; Park et al. 2008). In cultures of primary neurons derived from eEF2K-KO mice, general protein synthesis is not quantitatively different compared with WT cultures, but, as expected, the expression of Synapsin2b is increased, while the expression of MAP1b is decreased (however, we found no changes in eEF2 and TRIM3 levels).

In the hippocampus, eEF2K-KO mice showed a higher expression of Synapsin 2b (but no changes in MAP1b, eEF2, and TRIM3). Interestingly, these data correlate with a significantly higher density of synaptic vesicles at symmetric, GABAergic synapses of granule cells, which we did not observe at the presynaptic compartment of asymmetric, glutamatergic synapses. This (along with our electrophysiological data of eEF2K-KO mice) mirrors the ultrastructural/functional analysis of Synapsin 2 KO mice (Medrihan et al. 2013).

With 2 different approaches, we also strongly proved that the eEF2K activity-dependent modulation of Syn2b expression partially explains the ability of eEF2K to modulate presynaptic transmission: eEF2K overexpression is unable to modify mPSC frequency in neurons in which the expression of Syn2b is abolished with a specific Syn2b siRNA and the reduction in both mEPSC and mIPSC frequency, but not mIPSC amplitude, decay time, and area, induced by the overexpression of eEF2K were rescued by the co-expression of Syn2b. Since synapsins are involved in tethering synaptic vesicles to the actin-cytoskeleton (Hilfiker et al. 1999), higher Syn2b expression levels probably correlate with larger reserve pools of vesicles near the active zone.

Interestingly, the eEF2K-KO mice exhibit higher levels of $GABA_AR$-α5-subunit-mediated tonic inhibition, although we do not know how this occurs. It is noteworthy that the increase in tonic inhibition does not present itself under basal conditions but rather under conditions resembling a state of increased network activity. Possibly under baseline activity, the amount of diffusing GABA is not sufficient to unmask the difference of WT and eEF2K-KO mice with respect to extracellular $GABA_A$ receptors (Fig. 2*A*: current shift bicucculine vs. baseline does not differ between WT and eEF2K-KO mice). This might also explain why an increase in tonic inhibition (and the potentiated mIPSCs) in the DG that we observed in the eEF2K-KO mice is not enough to macroscopically change the EEG frequency bands or the spontaneously occurring EEG spikes in basal condition, but clearly do result in a reduced susceptibility to seizures (see below).

Thus, the eEF2K/eEF2 pathway tonically modulates inhibitory synapses by downregulating presynaptically the expression of synaptic vesicle-associated proteins like Syn2b and postsynaptically by downregulating the efficacy of $GABA_ARs$, including, but probably not limited to, the α5-subunit-containing $GABA_AR$.

eEF2K-KO Mice Are Less Susceptible to Seizures, Have a Specific Memory Impairment in the Hippocampus, and Genetic or Pharmacological Inhibition of eEF2K Activity Rescues the Epileptic Phenotype in a Mouse Model of Epilepsy

Given that eEF2K-KO mice exhibit a stronger GABAergic synaptic transmission and tonic inhibition in the dentate gyrus, we wanted to test whether they show behavioral abnormalities and whether they are protected from seizures.

Surprisingly, genetic deletion of eEF2K differentially affects the formation of hippocampal-dependent memories: spatial memory (MWM, reverse MWM, and novel place of object recognition) is normal; specifically only trace and contextual but not tone

fear conditioning are impaired. In addition, with a series of CTA experiments, we found that eEF2K is not necessary for cortical-dependent forms of learning.

We have previously shown that a knock-in mutation in eEF2K, which strongly reduces its activity, disrupts CTA memory retrieval and that peEF2 is critical for cortical-dependent taste learning formation (Gildish et al. 2012). A possible explanation for the conflicting observations between the previous and current findings is that eEF2K KI mice have residual activity of the eEF2K, which causes 30% of wild-type eEF2 phosphorylation, whereas there is no measurable peEF2 in the eEF2K-KO mice used in this study. Thus, the residual activity of eEF2K probably leads to a selective upregulation or downregulation of specific proteins whose normal expression is essential for the retrieval of CTA memory in the eEF2K KI mice, while in the eEF2K-KO mice another subset of proteins, such as Synapsin2b and the α5 $GABA_A$, is involved.

The role of the DG in trace fear-conditioning memory has been discussed extensively in literature. Trace fear-conditioning memory results in the upregulation of immediate early genes in the DG, as opposed to tone delay fear conditioning (Weitemier and Ryabinin 2004). In addition, genetic deletion of the δ subunit of the $GABA_A$ receptor in DG enhances the expression of trace fear conditioning but not tone delay fear conditioning (Wiltgen et al. 2005). Furthermore, selective reduction of the α5 $GABA_A$ receptor in the hippocampus facilitates trace fear conditioning, but not contextual fear conditioning or tone delay fear conditioning (Crestani et al. 2002). Interestingly, similarly to what we observed in the eEF2K-KO mice, it has been reported that manipulating DG cells and subsequently altering DG plasticity differentially impairs contextual and trace fear memory but spares spatial memory (Shors et al. 2002; Saxe et al. 2006). One possible explanation is that different molecular signaling and extra hippocampal circuitry subserve spatial learning, contextual, and trace fear conditioning (Cahill and McGaugh 1998; Bannerman et al. 2002; Mizuno and Giese 2005).

Considering that other studies demonstrate that deletions or mutations in key genes involved in regulating protein translation cause severe alterations in brain functions that change memory formation and cognitive properties (Buffington et al. 2014), it might be a surprise that the elimination of the eEF2K/eEF2 pathway showed a relatively mild behavioral phenotype. However, it is important to consider that the initiation phase, as opposed to elongation and termination, is generally regarded as the rate-limiting step and the major target for protein translational control. Nonetheless, our and other proteomic studies (Kenney, Genheden; et al. 2015) demonstrate that the eEF2K/eEF2 pathway does modulate the expression level of a small subset of neuronal proteins.

As we expected, eEF2K-KO mice are also clearly protected from seizures when induced by the chemoconvulsant substances PTZ or pilocarpine. We thus established a genetic model for chronic epilepsy, using Syn1-KO mice, which become epileptic at 2–3 months of age (Fig. 6*B*) (Cambiaghi et al. 2013). We used these mice, because they mimic the epileptic phenotype of humans carrying mutations in the SYN I gene very well (Fassio et al. 2011). Interestingly, we found that in these mice, the level of peEF2 is strongly elevated in the hippocampus. By crossing eEF2K-KO mice with these Syn1-KO mice, we provide clear evidence that the absence of eEF2K is protective for the Syn1-KO mice in regards to the epileptic phenotype. Similarly, the pharmacological inhibition of eEF2K with NH125 was able to normalize the elevated level of peEF2 and the epileptic phenotype in the Syn1-KO mice.

High levels of peEF2 were recently reported in a mouse model of Alzheimer's disease (Li et al. 2005) and in brain material of patients affected by Alzheimer's disease. This is reflected by the pathological activation of AMPK and the consequent activation of eEF2K (Ma et al. 2014). Thus, a similar mechanism might be evoked in the Syn1-KO mouse in which the overexcitation could generate a vicious cycle of ever-increasing network activity: chronically increased neuronal activity might lead to the activation of the eEF2K/eEF2 pathway and the subsequent dampening of the GABAergic synapses would further increase network activity, thereby aggravating the epilepsies in the Syn1-KO mice.

Interestingly, releasing the inhibition of protein translation elongation rate by genetic deletion of eEF2K, which results in complete dephosphorylation of eEF2, specifically affects synaptic transmission at the inhibitory synapse and contextual-trace fear memory (see above). Releasing some of the inhibition on translation initiation by knocking down the eIF2α kinase, PKR, results in network hyperexcitability and enhanced long-lasting synaptic plasticity (Zhu et al. 2011; Di Prisco et al. 2014). However, the phosphorylation of both eEF2 and eIF2α is required for mGluR-LTD (Park et al. 2008; Di Prisco et al. 2014). Thus, possibly in different neurons, divergent and convergent pathways are differentially regulated via the modulation of either protein translation initiation and elongation rates. A better understanding of region- and neuronal type-specific translation regulation is critical for clarifying the pathogenesis of both neurodevelopmental and neurodegenerative diseases (Bhattacharya et al. 2012; Gkogkas et al. 2013; Santini et al. 2013; Segev et al. 2013; Gkogkas et al. 2014; Segev et al. 2015).

Taken together, we discovered that eEF2K affects the excitation/inhibition balance, which is relevant for applied research on and treatment of paroxysmal disorders of the nervous system, including, but not limited to, seizures/status epilepticus and epilepsy (Klitgaard 2005; Maguire et al. 2005; Scimemi et al. 2005; Pavlov and Walker 2013). Indeed, our in vivo results point toward the possibility of targeting eEF2K activity in the context of epilepsy, raising the possibility to pharmacologically reduce seizure extension and/or duration or susceptibility in patients where overactivation of the eEF2K/eEF2 pathway might contribute to the severity of the disease. Although it remains to clarify whether chronic eEF2K manipulation causes deficits in some forms of memory, it is also true that currently a sizeable proportion of epileptic patients who cannot be treated satisfactorily with drugs are subjected to surgical removal of the epileptic focus, which has important consequences for brain function.

Supplementary Material

Supplementary material can be found at: http://www.cercor.oxfordjournals.org/.

Funding

This work was financially supported by Comitato Telethon Fondazione Onlus, grant GGP13187, Fondazione CARIPLO project number 2012-0593, Italian Institute of Technology, Seed Grant, Ministry of Health in the frame of ERA-NET NEURON, PNR-CNR Aging Program 2012–2014, and Italian Ministry for Research PRIN 2010–2011. C.H. was supported by SyMBaD (ITN MarieCurie, Grant Agreement no. 238608—7th Framework Programme of the EU). K.R. was supported by European Union Seventh Framework Program EUROSPIN (Contract HEALTH-F2-2009-241498), the German-Israeli Foundation DIP (RO3971/1-1), and Israel Science Foundation, ISF (1003/12) E.T. was supported by the Israeli Planning and Budgeting Committee Program Fellowships, the Ministry of Science and Technology Program Fellowships, and Israel Society for Neuroscience for outstanding PhD students. C.G.P.

was supported by Wellcome Trust, grant 086688. J.C. was supported by NIMH (1R01 MH096463-01A1) AND NINDS (1R01 NSW076517-01A1).

Notes

The NLGN1 antibody was a gift from Nils Brose (Max Planck Institute of Experimental Medicine, Göttingen, Germany). The Syn2 antibody was a gift from Paul Greengard (The Rockefeller University, NY, USA). Syn2b cDNA was kindly provided by George J. Augustine (Nanyang Technological University, Singapore, Singapore). The pUltra-hot vector was provided by M. A. S. Moore (Memorial Sloan-Kettering Cancer Center, New York, USA) via the web service Addgene. Further input was given by Elena Battaglioli, Emanuela Toffolo, Patrizia Rosa, Peter Scheiffele, Tobias Böckers, and Morgan Sheng. We thank Elisa Faggiani for technical support. We also thank Stephanie Heise for editing support. *Conflict of Interest*: None declared.

References

Andersen P, Sundberg SH, Sveen O, Wigström H. 1977. Specific long-lasting potentiation of synaptic transmission in hippocampal slices. Nature. 266:736–737.

Autry AE, Adachi M, Nosyreva E, Na ES, Los MF, Cheng PF, Kavalali ET, Monteggia LM. 2011. NMDA receptor blockade at rest triggers rapid behavioural antidepressant responses. Nature. 475:91–95.

Bannerman DM, Deacon RM, Offen S, Friswell J, Grubb M, Rawlins JN. 2002. Double dissociation of function within the hippocampus: spatial memory and hyponeophagia. Behav Neurosci. 116:884–901.

Belelovsky K, Elkobi A, Kaphzan H, Nairn AC, Rosenblum K. 2005. A molecular switch for translational control in taste memory consolidation. Eur J Neurosci. 22:2560–2568.

Belelovsky K, Kaphzan H, Elkobi A, Rosenblum K. 2009. Biphasic activation of the mTOR pathway in the gustatory cortex is correlated with and necessary for taste learning. J Neurosci. 29:7424–7431.

Ben-Ari Y, Cossart R. 2000. Kainate, a double agent that generates seizures: two decades of progress. Trends Neurosci. 23:580–587.

Bhattacharya A, Kaphzan H, Alvarez-Dieppa AC, Murphy JP, Pierre P, Klann E. 2012. Genetic removal of p70 S6 kinase 1 corrects molecular, synaptic, and behavioral phenotypes in fragile X syndrome mice. Neuron. 76:325–337.

Bourgeron T. 2015. From the genetic architecture to synaptic plasticity in autism spectrum disorder. Nat Rev Neurosci. 16:551–563.

Browne GJ, Proud CG. 2002. Regulation of peptide-chain elongation in mammalian cells. Eur J Biochem. 269:5360–5368.

Buffington SA, Huang W, Costa-Mattioli M. 2014. Translational control in synaptic plasticity and cognitive dysfunction. Annu Rev Neurosci. 37:17–38.

Cahill L, McGaugh JL. 1998. Mechanisms of emotional arousal and lasting declarative memory. Trends Neurosci. 21:294–299.

Cambiaghi M, Cursi M, Monzani E, Benfenati F, Comi G, Minicucci F, Valtorta F, Leocani L. 2013. Temporal evolution of neurophysiological and behavioral features of synapsin I/II/III triple knock-out mice. Epilepsy Res. 103:153–160.

Chen Y, Stevens B, Chang J, Milbrandt J, Barres BA, Hell JW. 2008. NS21: re-defined and modified supplement B27 for neuronal cultures. J Neurosci Methods. 171:239–247.

Chin LS, Li L, Ferreira A, Kosik KS, Greengard P. 1995. Impairment of axonal development and of synaptogenesis in hippocampal neurons of synapsin I-deficient mice. Proc Natl Acad Sci USA. 92:9230–9234.

Cingolani LA, Thalhammer A, Yu LM, Catalano M, Ramos T, Colicos MA, Goda Y. 2008. Activity-dependent regulation of synaptic AMPA receptor composition and abundance by beta3 integrins. Neuron. 58:749–762.

Costa-Mattioli M, Gobert D, Stern E, Gamache K, Colina R, Cuello C, Sossin W, Kaufman R, Pelletier J, Rosenblum K, et al. 2007. eIF2alpha phosphorylation bidirectionally regulates the switch from short- to long-term synaptic plasticity and memory. Cell. 129:195–206.

Crawley JN, Belknap JK, Collins A, Crabbe JC, Frankel W, Henderson N, Hitzemann RJ, Maxson SC, Miner LL, Silva AJ, et al. 1997. Behavioral phenotypes of inbred mouse strains: implications and recommendations for molecular studies. Psychopharmacology (Berl). 132:107–124.

Crestani F, Keist R, Fritschy JM, Benke D, Vogt K, Prut L, Blüthmann H, Möhler H, Rudolph U. 2002. Trace fear conditioning involves hippocampal alpha5 GABA(A) receptors. Proc Natl Acad Sci USA. 99:8980–8985.

Czerniawski J, Yoon T, Otto T. 2009. Dissociating space and trace in dorsal and ventral hippocampus. Hippocampus. 19:20–32.

Davidkova G, Carroll RC. 2007. Characterization of the role of microtubule-associated protein 1B in metabotropic glutamate receptor-mediated endocytosis of AMPA receptors in hippocampus. J Neurosci. 27:13273–13278.

Di Prisco GV, Huang W, Buffington SA, Hsu CC, Bonnen PE, Placzek AN, Sidrauski C, Krnjević K, Kaufman RJ, Walter P, et al. 2014. Translational control of mGluR-dependent long-term depression and object-place learning by eIF2α. Nat Neurosci. 17:1073–1082.

Elkobi A, Ehrlich I, Belelovsky K, Barki-Harrington L, Rosenblum K. 2008. ERK-dependent PSD-95 induction in the gustatory cortex is necessary for taste learning, but not retrieval. Nat Neurosci. 11:1149–1151.

Erbayat-Altay E, Yamada KA, Wong M, Thio LL. 2008. Increased severity of pentylenetetrazol induced seizures in leptin deficient ob/ob mice. Neurosci Lett. 433:82–86.

Farisello P, Boido D, Nieus T, Medrihan L, Cesca F, Valtorta F, Baldelli P, Benfenati F. 2013. Synaptic and extrasynaptic origin of the excitation/inhibition imbalance in the hippocampus of synapsin I/II/III knockout mice. Cereb Cortex. 23:581–593.

Fassio A, Patry L, Congia S, Onofri F, Piton A, Gauthier J, Pozzi D, Messa M, Defranchi E, Fadda M, et al. 2011. SYN1 loss-of-function mutations in autism and partial epilepsy cause impaired synaptic function. Hum Mol Genet. 20:2297–2307.

Franklin K, Paxinos G. 2008. The mouse brain in stereotaxic coordinates, 3rd ed. Amsterdam: Academic Press.

Gildish I, Manor D, David O, Sharma V, Williams D, Agarwala U, Wang X, Kenney JW, Proud CG, Rosenblum K. 2012. Impaired associative taste learning and abnormal brain activation in kinase-defective eEF2K mice. Learn Mem. 19:116–125.

Gilmartin MR, McEchron MD. 2005. Single neurons in the dentate gyrus and CA1 of the hippocampus exhibit inverse patterns of encoding during trace fear conditioning. Behav Neurosci. 119:164–179.

Gitler D, Takagishi Y, Feng J, Ren Y, Rodriguiz RM, Wetsel WC, Greengard P, Augustine GJ. 2004. Different presynaptic roles of synapsins at excitatory and inhibitory synapses. J Neurosci. 24:11368–11380.

Gkogkas C, Sonenberg N, Costa-Mattioli M. 2010. Translational control mechanisms in long-lasting synaptic plasticity and memory. J Biol Chem. 285:31913–31917.

Gkogkas CG, Khoutorsky A, Cao R, Jafarnejad SM, Prager-Khoutorsky M, Giannakas N, Kaminari A, Fragkouli A, Nader K, Price TJ, et al. 2014. Pharmacogenetic inhibition of

eIF4E-dependent Mmp9 mRNA translation reverses fragile X syndrome-like phenotypes. Cell Rep. 9:1742–1755.

Gkogkas CG, Khoutorsky A, Ran I, Rampakakis E, Nevarko T, Weatherill DB, Vasuta C, Yee S, Truitt M, Dallaire P, et al. 2013. Autism-related deficits via dysregulated eIF4E-dependent translational control. Nature. 493:371–377.

Glykys J, Mody I. 2007. Activation of GABAA receptors: views from outside the synaptic cleft. Neuron. 56:763–770.

Grabrucker AM, Knight MJ, Proepper C, Bockmann J, Joubert M, Rowan M, Nienhaus GU, Garner CC, Bowie JU, Kreutz MR, et al. 2011. Concerted action of zinc and ProSAP/Shank in synaptogenesis and synapse maturation. EMBO J. 30:569–581.

Heise C, Gardoni F, Culotta L, di Luca M, Verpelli C, Sala C. 2014. Elongation factor-2 phosphorylation in dendrites and the regulation of dendritic mRNA translation in neurons. Front Cell Neurosci. 8:35.

Hilfiker S, Pieribone VA, Czernik AJ, Kao HT, Augustine GJ, Greengard P. 1999. Synapsins as regulators of neurotransmitter release. Philos Trans R Soc Lond B Biol Sci. 354:269–279.

Hoeffer CA, Cowansage KK, Arnold EC, Banko JL, Moerke NJ, Rodriguez R, Schmidt EK, Klosi E, Chorev M, Lloyd RE, et al. 2011. Inhibition of the interactions between eukaryotic initiation factors 4E and 4G impairs long-term associative memory consolidation but not reconsolidation. Proc Natl Acad Sci USA. 108:3383–3388.

Holt CE, Schuman EM. 2013. The central dogma decentralized: new perspectives on RNA function and local translation in neurons. Neuron. 80:648–657.

Huttner W, Schiebler W, Greengard P, DeCamilli P. 1983. Synapsin I (protein I), a nerve terminal-specific phosphoprotein. III. Its association with synaptic vesicles studied in a highly purified synaptic vesicle preparation. J Cell Biol. 5:1374–1388.

Im HI, Nakajima A, Gong B, Xiong X, Mamiya T, Gershon ES, Zhuo M, Tang YP. 2009. Post-training dephosphorylation of eEF-2 promotes protein synthesis for memory consolidation. PLoS One. 4:e7424.

Jelenković A, Jovanović M, Ninković M, Maksimović M, Bokonjić D, Bosković B. 2002. Nitric oxide (NO) and convulsions induced by pentylenetetrazol. Ann N Y Acad Sci. 962:296–305.

Jinde S, Zsiros V, Jiang Z, Nakao K, Pickel J, Kohno K, Belforte JE, Nakazawa K. 2012. Hilar mossy cell degeneration causes transient dentate granule cell hyperexcitability and impaired pattern separation. Neuron. 76:1189–1200.

Kenney JW, Genheden M, Moon KM, Wang X, Foster LJ, Proud CG. 2015. Eukaryotic elongation factor 2 kinase regulates the synthesis of microtubule-related proteins in neurons. J Neurochem. 136:276–284.

Kenney JW, Sorokina O, Genheden M, Sorokin A, Armstrong JD, Proud CG. 2015. Dynamics of elongation factor 2 kinase regulation in cortical neurons in response to synaptic activity. J Neurosci. 35:3034–3047.

Klitgaard H. 2005. Antiepileptic drug discovery: lessons from the past and future challenges. Acta Neurol Scand Suppl. 181:68–72.

Kopanitsa MV, Afinowi NO, Grant SG. 2006. Recording long-term potentiation of synaptic transmission by three-dimensional multi-electrode arrays. BMC Neurosci. 7:61.

Li L, Chin LS, Shupliakov O, Brodin L, Sihra TS, Hvalby O, Jensen V, Zheng D, McNamara JO, Greengard P. 1995. Impairment of synaptic vesicle clustering and of synaptic transmission, and increased seizure propensity, in synapsin I-deficient mice. Proc Natl Acad Sci USA. 92:9235–9239.

Li X, Alafuzoff I, Soininen H, Winblad B, Pei JJ. 2005. Levels of mTOR and its downstream targets 4E-BP1, eEF2, and eEF2 kinase in relationships with tau in Alzheimer's disease brain. FEBS J. 272:4211–4220.

Lois C, Hong EJ, Pease S, Brown EJ, Baltimore D. 2002. Germline transmission and tissue-specific expression of transgenes delivered by lentiviral vectors. Science. 295:868–872.

Ma T, Chen Y, Vingtdeux V, Zhao H, Viollet B, Marambaud P, Klann E. 2014. Inhibition of AMP-activated protein kinase signaling alleviates impairments in hippocampal synaptic plasticity induced by amyloid β. J Neurosci. 34:12230–12238.

Maguire JL, Stell BM, Rafizadeh M, Mody I. 2005. Ovarian cycle-linked changes in GABA(A) receptors mediating tonic inhibition alter seizure susceptibility and anxiety. Nat Neurosci. 8:797–804.

Manfredi I, Zani AD, Rampoldi L, Pegorini S, Bernascone I, Moretti M, Gotti C, Croci L, Consalez GG, Ferini-Strambi L, et al. 2009. Expression of mutant beta2 nicotinic receptors during development is crucial for epileptogenesis. Hum Mol Genet. 18:1075–1088.

Mann M. 2006. Functional and quantitative proteomics using SILAC. Nat Rev Mol Cell Biol. 7:952–958.

McCamphill PK, Farah CA, Anadolu MN, Hoque S, Sossin WS. 2015. Bidirectional regulation of eEF2 phosphorylation controls synaptic plasticity by decoding neuronal activity patterns. J Neurosci. 35:4403–4417.

Medrihan L, Cesca F, Raimondi A, Lignani G, Baldelli P, Benfenati F. 2013. Synapsin II desynchronizes neurotransmitter release at inhibitory synapses by interacting with presynaptic calcium channels. Nat Commun. 4:1512.

Mizuno K, Giese KP. 2005. Hippocampus-dependent memory formation: do memory type-specific mechanisms exist? J Pharmacol Sci. 98:191–197.

Moore CE, Mikolajek H, Regufe da Mota S, Wang X, Kenney JW, Werner JM, Proud CG. 2015. Elongation factor 2 kinase is regulated by proline hydroxylation and protects cells during hypoxia. Mol Cell Biol. 35:1788–1804.

Naldini L, Blomer U, Gallay P, Ory D, Mulligan R, Gage FH, Verma IM, Trono D. 1996. In vivo gene delivery and stable transduction of nondividing cells by a lentiviral vector. Science. 272:263–267.

Nosten-Bertrand M, Kappeler C, Dinocourt C, Denis C, Germain J, Phan Dinh Tuy F, Verstraeten S, Alvarez C, Métin C, Chelly J, et al. 2008. Epilepsy in Dcx knockout mice associated with discrete lamination defects and enhanced excitability in the hippocampus. PLoS One. 3:e2473.

Nosyreva E, Szabla K, Autry AE, Ryazanov AG, Monteggia LM, Kavalali ET. 2013. Acute suppression of spontaneous neurotransmission drives synaptic potentiation. J Neurosci. 33:6990–7002.

Ounallah-Saad H, Sharma V, Edry E, Rosenblum K. 2014. Genetic or pharmacological reduction of PERK enhances cortical-dependent taste learning. J Neurosci. 34:14624–14632.

Park S, Park JM, Kim S, Kim JA, Shepherd JD, Smith-Hicks CL, Chowdhury S, Kaufmann W, Kuhl D, Ryazanov AG, et al. 2008. Elongation factor 2 and fragile X mental retardation protein control the dynamic translation of Arc/Arg3.1 essential for mGluR-LTD. Neuron. 59:70–83.

Pavlov I, Walker MC. 2013. Tonic GABA(A) receptor-mediated signalling in temporal lobe epilepsy. Neuropharmacology. 69:55–61.

Pierson JL, Pullins SE, Quinn JJ. 2015. Dorsal hippocampus infusions of CNQX into the dentate gyrus disrupt expression of trace fear conditioning. Hippocampus. 25:779–785.

Pietersen AN, Patel N, Jefferys JG, Vreugdenhil M. 2009. Comparison between spontaneous and kainate-induced gamma

oscillations in the mouse hippocampus in vitro. Eur J Neurosci. 29:2145–2156.

Pyr Dit Ruys S, Wang X, Smith EM, Herinckx G, Hussain N, Rider MH, Vertommen D, Proud CG. 2012. Identification of autophosphorylation sites in eukaryotic elongation factor-2 kinase. Biochem J. 442:681–692.

Rodriguez P, Levy WB. 2001. A model of hippocampal activity in trace conditioning: where's the trace? Behav Neurosci. 115:1224–1238.

Rosahl TW, Spillane D, Missler M, Herz J, Selig DK, Wolff JR, Hammer RE, Malenka RC, Südhof TC. 1995. Essential functions of synapsins I and II in synaptic vesicle regulation. Nature. 375:488–493.

Rosenberg T, Gal-Ben-Ari S, Dieterich DC, Kreutz MR, Ziv NE, Gundelfinger ED, Rosenblum K. 2014. The roles of protein expression in synaptic plasticity and memory consolidation. Front Mol Neurosci. 7:86.

Rosenblum K, Meiri N, Dudai Y. 1993. Taste memory: the role of protein synthesis in gustatory cortex. Behav Neural Biol. 59:49–56.

Ryazanov AG. 2002. Elongation factor-2 kinase and its newly discovered relatives. FEBS Lett. 514:26–29.

Ryazanov AG, Shestakova EA, Natapov PG. 1988. Phosphorylation of elongation factor 2 by EF-2 kinase affects rate of translation. Nature. 334:170–173.

Sala C, Segal M. 2014. Dendritic spines: the locus of structural and functional plasticity. Physiol Rev. 94:141–188.

Sala M, Braida D, Lentini D, Busnelli M, Bulgheroni E, Capurro V, Finardi A, Donzelli A, Pattini L, Rubino T, et al. 2011. Pharmacologic rescue of impaired cognitive flexibility, social deficits, increased aggression, and seizure susceptibility in oxytocin receptor null mice: a neurobehavioral model of autism. Biol Psychiatry. 69:875–882.

Santini E, Huynh TN, MacAskill AF, Carter AG, Pierre P, Ruggero D, Kaphzan H, Klann E. 2013. Exaggerated translation causes synaptic and behavioural aberrations associated with autism. Nature. 493:411–415.

Saxe MD, Battaglia F, Wang JW, Malleret G, David DJ, Monckton JE, Garcia AD, Sofroniew MV, Kandel ER, Santarelli L, et al. 2006. Ablation of hippocampal neurogenesis impairs contextual fear conditioning and synaptic plasticity in the dentate gyrus. Proc Natl Acad Sci USA. 103:17501–17506.

Scheetz AJ, Nairn AC, Constantine-Paton M. 1997. N-methyl-D-aspartate receptor activation and visual activity induce elongation factor-2 phosphorylation in amphibian tecta: a role for N-methyl-D-aspartate receptors in controlling protein synthesis. Proc Natl Acad Sci USA. 94:14770–14775.

Scheetz AJ, Nairn AC, Constantine-Paton M. 2000. NMDA receptor-mediated control of protein synthesis at developing synapses. Nat Neurosci. 3:211–216.

Schmeisser MJ, Ey E, Wegener S, Bockmann J, Stempel AV, Kuebler A, Janssen AL, Udvardi PT, Shiban E, Spilker C, et al. 2012. Autistic-like behaviours and hyperactivity in mice lacking ProSAP1/Shank2. Nature. 486:256–260.

Schmidt EK, Clavarino G, Ceppi M, Pierre P. 2009. SUnSET, a nonradioactive method to monitor protein synthesis. Nat Methods. 6:275–277.

Schwartzkroin PA, Wester K. 1975. Long-lasting facilitation of a synaptic potential following tetanization in the in vitro hippocampal slice. Brain Res. 89:107–119.

Scimemi A, Semyanov A, Sperk G, Kullmann DM, Walker MC. 2005. Multiple and plastic receptors mediate tonic GABAA receptor currents in the hippocampus. J Neurosci. 25:10016–10024.

Segev Y, Barrera I, Ounallah-Saad H, Wibrand K, Sporild I, Livne A, Rosenberg T, David O, Mints M, Bramham CR, et al. 2015. PKR inhibition rescues memory deficit and ATF4 overexpression in ApoE ε4 human replacement mice. J Neurosci. 35:12986–12993.

Segev Y, Michaelson DM, Rosenblum K. 2013. ApoE ε4 is associated with eIF2α phosphorylation and impaired learning in young mice. Neurobiol Aging. 34:863–872.

Shors TJ, Townsend DA, Zhao M, Kozorovitskiy Y, Gould E. 2002. Neurogenesis may relate to some but not all types of hippocampal-dependent learning. Hippocampus. 12:578–584.

Sutton MA, Ito HT, Cressy P, Kempf C, Woo JC, Schuman EM. 2006. Miniature neurotransmission stabilizes synaptic function via tonic suppression of local dendritic protein synthesis. Cell. 125:785–799.

Sutton MA, Taylor AM, Ito HT, Pham A, Schuman EM. 2007. Postsynaptic decoding of neural activity: eEF2 as a biochemical sensor coupling miniature synaptic transmission to local protein synthesis. Neuron. 55:648–661.

Taha E, Gildish I, Gal-Ben-Ari S, Rosenblum K. 2013. The role of eEF2 pathway in learning and synaptic plasticity. Neurobiol Learn Mem. 105:100–106.

Toader O, Forte N, Orlando M, Ferrea E, Raimondi A, Baldelli P, Benfenati F, Medrihan L. 2013. Dentate gyrus network dysfunctions precede the symptomatic phase in a genetic mouse model of seizures. Front Cell Neurosci. 7:138.

Treviño M, Vivar C, Gutiérrez R. 2007. Beta/gamma oscillatory activity in the CA3 hippocampal area is depressed by aberrant GABAergic transmission from the dentate gyrus after seizures. J Neurosci. 27:251–259.

Vaccaro P, Dente L, Onofri F, Zucconi A, Martinelli S, Valtorta F, Greengard P, Cesareni G, Benfenati F. 1997. Anti-synapsin monoclonal antibodies: epitope mapping and inhibitory effects on phosphorylation and Grb2 binding. Brain Res Mol Brain Res. 52:1–16.

Verpelli C, Piccoli G, Zanchi A, Gardoni F, Huang K, Brambilla D, Di Luca M, Battaglioli E, Sala C. 2010. Synaptic activity controls dendritic spine morphology by modulating eEF2-dependent BDNF synthesis. J Neurosci. 30:5830–5842.

Vezzani A. 2009. Pilocarpine-induced seizures revisited: what does the model mimic? Epilepsy Curr 9:146–148.

Vorhees CV, Williams MT. 2006. Morris water maze: procedures for assessing spatial and related forms of learning and memory. Nat Protoc. 1:848–858.

Weitemier AZ, Ryabinin AE. 2004. Subregion-specific differences in hippocampal activity between Delay and Trace fear conditioning: an immunohistochemical analysis. Brain Res. 995:55–65.

Williams BJ, Bimonte-Nelson HA, Granholm-Bentley AC. 2006. ERK-mediated NGF signaling in the rat septo-hippocampal pathway diminishes with age. Psychopharmacology (Berl). 188:605–618.

Wiltgen BJ, Sanders MJ, Ferguson C, Homanics GE, Fanselow MS. 2005. Trace fear conditioning is enhanced in mice lacking the delta subunit of the GABAA receptor. Learn Mem. 12:327–333.

Zhu PJ, Huang W, Kalikulov D, Yoo JW, Placzek AN, Stoica L, Zhou H, Bell JC, Friedlander MJ, Krnjević K, et al. 2011. Suppression of PKR promotes network excitability and enhanced cognition by interferon-γ-mediated disinhibition. Cell. 147:1384–1396.